Author/s:
Lindblom, RSJ;Higgins, GC;Nguyen, TV;Arnstein, M;Henstridge, DC;Granata, C;Snelson, M;Thallas-Bonke, V;Cooper, ME;Forbes, JM;Coughlan, MT

Title:
Delineating a role for the mitochondrial permeability transition pore in diabetic kidney disease by targeting cyclophilin D

Date:
2020-01-01

Citation:
Lindblom, R. S. J., Higgins, G. C., Nguyen, T. V., Arnstein, M., Henstridge, D. C., Granata, C., Snelson, M., Thallas-Bonke, V., Cooper, M. E., Forbes, J. M. & Coughlan, M. T. (2020). Delineating a role for the mitochondrial permeability transition pore in diabetic kidney disease by targeting cyclophilin D. Clinical Science, 134 (2), pp.239-259. https://doi.org/10.1042/CS20190787.

Persistent Link:
https://hdl.handle.net/11343/299780

Clinical Science (2020) **134** 239–259
https://doi.org/10.1042/CS20190787

PORTLAND PRESS

Research Article

Delineating a role for the mitochondrial permeability transition pore in diabetic kidney disease by targeting cyclophilin D

Runa S.J. Lindblom[1], Gavin C. Higgins[1,2], Tuong-Vi Nguyen[2], Maryann Arnstein[1], Darren C. Henstridge[2], Cesare Granata[1], Matthew Snelson[1], Vicki Thallas-Bonke[2], Mark E. Cooper[1], Josephine M. Forbes[3] and Melinda T. Coughlan[1,2]

[1]Department of Diabetes, Central Clinical School, Alfred Medical Research and Education Precinct, Monash University, Melbourne, Victoria, Australia; [2]Baker Heart & Diabetes Institute, Melbourne, Victoria, Australia; [3]Glycation and Diabetes Group, Mater Research Institute, Translational Research Institute, The University of Queensland, Woolloongabba, Queensland, Australia

Correspondence: Runa Lindblom (runa.lindblom@monash.edu)

Mitochondrial stress has been widely observed in diabetic kidney disease (DKD). Cyclophilin D (CypD) is a functional component of the mitochondrial permeability transition pore (mPTP) which allows the exchange of ions and solutes between the mitochondrial matrix to induce mitochondrial swelling and activation of cell death pathways. CypD has been successfully targeted in other disease contexts to improve mitochondrial function and reduced pathology. Two approaches were used to elucidate the role of CypD and the mPTP in DKD. Firstly, mice with a deletion of the gene encoding CypD (*Ppif*$^{-/-}$) were rendered diabetic with streptozotocin (STZ) and followed for 24 weeks. Secondly, Alisporivir, a CypD inhibitor was administered to the db/db mouse model (5 mg/kg/day oral gavage for 16 weeks). *Ppif*$^{-/-}$ mice were not protected against diabetes-induced albuminuria and had greater glomerulosclerosis than their WT diabetic littermates. Renal hyperfiltration was lower in diabetic *Ppif*$^{-/-}$ as compared with WT mice. Similarly, Alisporivir did not improve renal function nor pathology in db/db mice as assessed by no change in albuminuria, KIM-1 excretion and glomerulosclerosis. Db/db mice exhibited changes in mitochondrial function, including elevated respiratory control ratio (RCR), reduced mitochondrial H_2O_2 generation and increased proximal tubular mitochondrial volume, but these were unaffected by Alisporivir treatment. Taken together, these studies indicate that CypD has a complex role in DKD and direct targeting of this component of the mPTP will likely not improve renal outcomes.

Introduction

Chronic kidney disease (CKD) is recognised as a leading cause of morbidity and mortality amongst the 425 million people estimated to have diabetes globally [1]. This represents a significant burden to healthcare systems as the number of people with all types of diabetes is projected to rise over the next few decades [1]. Currently, best practice clinical management involves strict glucose control and blood pressure reduction to alleviate risk for progression to end stage renal disease. Although these approaches can successfully stabilise the rate of progression in many patients, they do not entirely eliminate disease or risk for renal replacement therapy [2,3]. There remains an urgent need for new therapeutic approaches in targeting diabetic kidney disease (DKD) and a requirement to deepen our understanding of the aetiology and pathogenesis to improve patient outcomes.

The therapeutic potential of maintaining and/or restoring mitochondrial 'health' is currently being investigated in DKD, since a decline in mitochondrial function is associated with renal functional decline

Received: 31 July 2019
Revised: 10 January 2020
Accepted: 16 January 2020

Accepted Manuscript Online: 16 January 2020
Version of Record published: 29 January 2020

Clinical Science (2020) **134** 239–259
https://doi.org/10.1042/CS20190787

and injury [4]. Mitochondria are considered vital for the function of nephrons which consume high levels of oxygen and adenosine triphosphate (ATP) to support the metabolic demands of selective reabsorption in the proximal and distal tubules [5,6]. Furthermore, mitochondria play an important role in adaptation to the metabolic changes and hypoxia associated with diabetic renal pathophysiology [6,7]. Thus, a suite of mitochondria-targeted compounds are currently being developed and tested in pre-clinical models to determine their efficacy in the treatment of DKD. One potential target for therapy is the mitochondrial permeability transition pore (mPTP), which is a stress-sensitive pore that traverses both the inner and outer mitochondrial membranes. Transient mPTP opening is thought to dissipate chemical and electrical ion build up from the mitochondrial matrix to the cytosol to restore ionic balance [8,9]. However, persistent opening of the mPTP results in mitochondrial swelling and subsequent outer membrane rupture, along with a concomitant decline in capacity for oxidative phosphorylation (OXPHOS) [10]. Inappropriate mPTP opening is associated with necrotic cell death as the maintenance of ATP production is necessary for the energy demanding process of apoptosis [11,12]. Previous preclinical studies of DKD have shown increased mPTP opening events occur in kidney mitochondria, which coincided with the development of renal morphological injury and a decline in renal cortical mitochondrial respiratory chain function in a rat model of streptozotocin (STZ)-induced diabetes [4].

Although the exact mechanism that enables trafficking through the mPTP is still under debate, newer models suggest several key membrane proteins are involved in pore opening. This includes the outer membrane pore-forming proteins Bax and Bak, the F1alpha unit of ATP synthase, and cyclophilin D (CypD) [13,14]. CypD is considered to regulate pore opening and it therefore remains as a unique target which can be directly inhibited by broad spectrum immunosuppressants such as cyclosporine A (CsA) and its newer non-immunosuppressive analogue Alisporivir (Debio025) [15,16]. In the kidney, CypD deletion in mice is protective against the development of renal fibrosis and proximal tubular epithelial cell (PTEC) damage following unilateral ureteral obstruction, and ischemia reperfusion injury [17–19]. However, the effects of targeting CypD on DKD progression have not been investigated. The present study aims to investigate the role of CypD in DKD by utilising two disparate yet complementary approaches. Firstly, mice with a global genetic knock out (KO) of the peptidylprolyl isomerase F gene, *Ppif*, (which is the gene encoding for CypD), and secondly using pharmacological inhibition by Alisporivir in a murine model of experimental diabetes.

Experimental

Mouse studies

All animal studies were approved by the Alfred Medical Research and Education Precinct Animal Ethics Committee and the National Health and Medical Research Council of Australia. All procedures were performed in accordance with the Australian code of conduct for ethical research involving animals. All animals were housed at the Alfred Medical Research and Education Precinct Animal Centre, Melbourne, Australia, and were maintained following established ethical procedures, in a temperature controlled environment at 22°C with a 12 h light/dark cycle with *ad libitum* access to rodent chow (standard mouse chow, Specialty Feeds, Perth, WA, Australia) and water.

Ppif$^{-/-}$ mouse studies

Six week old Male C57BL/6 mice with a global deletion of Cyp D (*Ppif* $^{-/-}$) were purchased from the Jackson Laboratory (Bar Harbor, ME, U.S.A.). Diabetes was induced at 6 weeks of age (n=15 mice per group, $Ppif^{WT/WT}$ STZ or $Ppif^{-/-}$ STZ) by five daily intraperitoneal injections of low dose STZ (55 mg/kg, Sigma-Aldrich, St Louis, MO), with control mice receiving the vehicle, sodium citrate buffer (CIT) alone (n=15 mice per group, $Ppif^{WT/WT}$ or $Ppif^{-/-}$). After 10 days, plasma glucose concentrations were determined to confirm diabetes development and mice with blood glucose not exceeding >15 mmol/l glucose (observed in >98% of mice) were excluded from the study. None of the animals with diabetes required exogenous insulin supplementation to maintain body weight or to prevent ketosis.

At 20 weeks after induction of diabetes, mice were placed individually into metabolic cages (Iffa Credo, L'Arbresele, France) for 24 h. Urine and plasma from submandibular collections were stored at −80°C for subsequent analysis. Blood glucose was monitored using a glucometer (Accutrend; Boehringer Manheim Biochemica, Manheim, Germany). Glycated haemoglobin (GHb) was determined by turbidimetric inhibition immunoassay using a Cobas Integra 400 autoanalyzer (Roche Diagnostics Corporation, U.S.A.) in lysates of erythrocytes separated from whole blood. After 22 weeks, animals were killed by sodium pentobarbitone intraperitoneally (100 mg/kg body weight) (Euthatal; Sigma-Aldrich, Castle Hill, NSW, Australia) followed by cardiac exsanguination. The kidneys were rapidly dissected, weighed, and snap-frozen or placed in 10% (v/v) neutral buffered formalin for fixation before paraffin embedding. In a subset of mice (n=5 per group), mitochondria were isolated from renal cortices as later described.

Pharmacological inhibition of cyclophilin D

Male *db/db* mice (C57*BKS.Cg-Dock7*$^{m+/+}$*Lepr*^{db}*/J)* and their *db/m* littermate controls were obtained from colonies maintained at the Alfred Medical Research and Education Precinct Animal Services (Melbourne, Australia). Mice were randomly assigned at 7 weeks of age to either vehicle (10% Cremophor EL in water) or Alisporivir (Novartis, Basel, Switzerland) at 5 mg/kg/day by oral gavage. Animals were treated for 16 weeks with blood glucose and body weight assessed weekly. Any animal which lost 20% of body weight or developed severe ketoacidosis during the study was excluded before endpoint in accordance with ethical guidelines. HbA_{1c} was determined using the Cobas b 101 system (Roche diagnostics, IN, U.S.A.). At week 15, body composition was determined using an EchoMRI (EchoMRI™, Houston, TX, U.S.A.) and mice were placed into individual Comprehensive Laboratory Animal Monitoring System (CLAMS, Columbus Instruments, Columbus, Ohio, U.S.A.) chambers to determine physical activity and respiration by indirect calorimetry as previously described in full [20]. Metabolic caging to collect 24 h urine samples was performed at 8 weeks (midpoint) and 15 weeks (endpoint). Mice were killed and kidneys were harvested and processed as described above. Additionally, mitochondria were isolated from the whole cortex of the left kidney for all animals (described below). A small section of renal cortex was also reserved for transmission electron micrography (described below).

Renal function and morphometry

The 24-h urinary albumin excretion rates were determined using a mouse-specific sandwich ELISA in timed urine collections (Bethyl Laboratories, Montgomery, TX, U.S.A.) according to the manufacturer's instructions. Creatinine was assessed in both plasma and urine samples using commercially available kits for the Cobas Integra 400 autoanalyzer (Roche Diagnostics, IN, U.S.A.). Plasma cystatin C was measured using ELISA (R&D Systems Inc., Minneapolis MN, U.S.A.). Urinary content of kidney injury molecule (KIM)-1 was measured using a commercially available sandwich ELISA (USCN Life Sciences, Wuhan, China) according to the kit protocol. Glomerular sclerosis index (GSI) was assessed in 3-μm paraffin embedded periodic acid Schiff (PAS) stained sections by a semi-quantitative method as previously described [21]. Paraffin sections of kidneys were used to stain for collagen type IV (Col IV) using a goat polyclonal collagen IV antibody (Southern Biotech, Birmingham, AL, U.S.A.) [22].

Mitochondrial isolation

Freshly collected kidney cortex was minced on ice and placed into 1 ml of ice-cold Isolation Buffer (IsoB) (70 mM sucrose; 210 mM D-mannitol; 5 mM HEPES; 1 mM EGTA; 0.5% (w/v) fatty acid free bovine serum albumin [Sigma-Aldrich, NSW, Australia]) followed by 6–8 careful strokes in a Potter–Elvehjem homogenizer set in an ice-bath. Lysate was then collected and any remaining tissue homogenised with an additional 1 ml IsoB for 2–3 more strokes. The lysate underwent differential centrifugation at 4°C as previously described [23]. Briefly, ∼2 ml total volume was centrifuged for 5 min at 800 ***g***. Supernatant was collected and centrifuged at 8000 ***g*** ×10 min. Mitochondrial pellet was washed in 500 μl IsoB and centrifuged again at 8000 ***g*** × 10 min. Final pellet was resuspended in 115 μl IsoB and stored on ice for use in functional assays (below). Total protein was determined by the bicinchoninic acid method and corrected for background protein in IsoB (Pierce-Thermo Fisher Scientific, Melbourne, Australia).

Mitochondrial oxygen consumption

Mitochondria were resuspended in mitochondrial assay buffer (MAS) (70 mM sucrose; 220 mM D-mannitol; 10 mM KH_2PO4; 5 mM $MgCl_2 \cdot 6H_2O$; 2 mM HEPES; 1 mM EGTA; 0.2% (w/v) fatty acid free bovine serum albumin, pH 7.2) and loaded into a XFe96well Seahorse Bioanalyzer plate (Seahorse Bioscience, Agilent, Santa Clara CA, U.S.A.) with a minimum of five replicate wells per mouse. For complex I respiration 10 μg of mitochondria was loaded per well with 0.5 mM glutamate and 0.5 mM malate. Plates were centrifuged at 2000***g*** for 20 min at 4°C before adding substrates and then immediately loaded into the XFe96 Seahorse machine. Basal respiration with substrates was measured twice for 3 min each, followed by subsequent injections of (A) 0.5 mM ADP (State 3o), (B) 2.5 μg/μl oligomycin (State 4), (C) 1 μM carbonyl cyanide trifluoromethoxyphenylhydrazone (FCCP) (State 3u) and (D) 4 μM antimycin-A. Data were analysed per individual mouse with each injection point assessed for successful response via pre-defined criteria. Injection measurements were excluded where oxygen consumption was reduced to 0 pmol/min, or where the compounds did not perform as expected for that individual replicate (e.g. no response to oligomycin). The average value of remaining replicates was used. Individual animals were excluded where ADP injection did not increase oxygen consumption rate (OCR).

Clinical Science (2020) **134** 239–259
https://doi.org/10.1042/CS20190787

Hydrogen peroxide production

Hydrogen peroxide (H_2O_2) production in renal cortical mitochondrial preparations was measured by fluorescence using the Amplex Red reagent (Molecular Probes, Invitrogen). In addition, H_2O_2 production was assessed in the presence of 10 mM glutamate and 10 mM malate for complex I, or, 10 mM succinate for complex II, plus 5 μM rotenone (a complex I inhibitor). Results were then normalised to no substrates group to determine effects of complex I and II stimulation.

Mitochondrial swelling assay

The induction of mitochondrial permeability transition (mPT) in mouse kidney mitochondria was monitored by absorbance changes at 540 nm based on a microtiter plate procedure developed by Waldmeier et al. [15], with the following modifications. Mitochondria, isolated by differential centrifugation as described above were washed twice and resuspended in energised respiratory buffer (ERB) (210 mM mannitol, 70 mM sucrose, 5mM HEPES, 5 mM glutamate, 5 mM malate, 0.05 M Tris, pH 7.4). Mitochondrial protein, 100 μg, was added to each well in 110 μl ERB, then incubated with 10 μM CsA or ERB control where appropriate for 5 min before the addition of 5 μl of calcium solution (2.5 mM $CaCl_2 \cdot 2H_2O$, 1 mM K_2HPO_4) or ERB. Total volume = 125 μl per well. Δabsorbance was determined over 10 min with a microtiter plate reader (*Ppif* study) or 15 min (*db/db* study) using an EnSpire multimode plate reader (Perkin Elmer, Waltham, MA, U.S.A.).

Quantitative reverse transcription-polymerase chain reaction

RNA was isolated from kidney cortex (20–30mg) using TRIzol Reagent (Life Technologies). Contaminating DNA was removed after treatment with DNA-free DNAse according to the manufacturer's specifications (Ambion Inc, Austin, U.S.A.). DNA-free RNA was reverse transcribed into cDNA using the Superscript First Strand Synthesis System according to the manufacturer's specifications (Life Technologies BRL, Grand Island, NY). Real-time PCR was performed using SYBR green PCR mix (Applied Biosystems, primer concentration of 500 nM) or Taqman PCR kit (18S rRNA TaqMan Control Reagent kit, ABI Prism 7500; Perkin-Elmer) using a 7500 Fast Real-time PCR System (Applied Biosystem, VIC, Australia), and normalized relative to 18S ribosomal RNA. All values are presented as fold change relative to $Ppif^{WT/WT}$ CIT control or *db/m* vehicle control. The nucleotide sequences for primers examined are shown in Supplementary Table S1.

Citrate synthase activity

Citrate synthase activity was assayed as previously described via colorimetric release of acetyl coenzyme A in the presence of DTNB 5,5-dithiobis-2-nitrobenzoate [24]. Calculated activity levels were then normalised to total mitochondrial isolation protein concentrations.

Transmission electron microscopy and analysis of mitochondrial morphology

Mitochondrial morphology (length and width) was determined in electron micrographs of proximal tubule epithelial cells. Immediately following exsanguination, renal cortices were fixed in 2.5% glutaraldehyde in 0.1 M sodium cacodylate buffer and tissue was processed for standard transmission electron microscopy using post-fixation in 1% OsO_4 and embedded in Epon resin. Ultrathin sections were cut and stained with lead citrate and uranyl acetate and imaged on a Hitachi H-7500 transmission electron microscope equipped with a Gatan Multiscan 791 CCD camera. Up to 10 images of proximal tubule epithelial cells per kidney section were randomly collected for each mouse at ×8000 magnification. Image field size was 17.44 × 17.44 μm each. Individual complete mitochondria were circled by hand for a subset of n=3 mice per group. Mitochondria in each image per mouse were hand circled and measured with (Fiji Is Just) ImageJ software and values used to calculate Form Factor (length/width) as previously described [25]. In addition, the 2D volume of mitochondria within each field per section were measured and expressed as mitochondrial percentage area per mm^2 cytosol. For purpose of cytosolic area determination nuclei, brush borders, and non-proximal tubular structures were excluded. Cumulative results for each mouse were used to express mean volume and aspect ratio per group.

Western immunoblotting

Immunoblotting was performed as previously described with minor modifications [26]. Briefly, 8 μg of isolated mitochondria were lysed by three freeze-thaw cycles and separated by electrophoresis on 4–20% Mini-Protean TGX Stain-Free Gel (Bio-Rad laboratories, Gladesville, NSW, Australia), transferred to polyvinylidene fluoride (PVDF)

Table 1 Phenotypic and metabolic characteristics of wild-type (WT) and *Ppif*$^{-/-}$ (KO) mice

	CIT		STZ		Two-way ANOVA			
	WT	KO	WT	KO	WT vs KO		CIT vs STZ	
	Mean ± SD	Mean ± SD	Mean ± SD	Mean ± SD	CIT	STZ	WT	KO
Body weight (g)	34.9 ± 3.3	31.9 ± 3.7	24.3 ± 3.0	24.6 ± 3.3	*	ns	****	****
Fasting blood glucose at cull (mmol/l)	14.2 ± 3.5	13.0 ± 2.8	29.5 ± 4.2	27.9 ± 6.4	ns	ns	****	****
Total kidney weight (g)	0.39 ± 0.04	0.38 ± 0.05	0.47 ± 0.07	0.434 ± 0.06	ns	ns	****	*
Kidney:body weight ratio (mg/kg)	11.1 ± 1.2	11.9 ± 1.4	19.6 ± 3.2	17.9 ± 3.4	ns	ns	****	****
24 h metcaging								
12 weeks								
Urine (ml)	0.6 ± 0.4	0.6 ± 0.4	14.9 ± 6.8	10.9 ± 7.3	ns	*	****	****
H_2O (ml)	4.7 ± 2.1	4.7 ± 1.5	18.8 ± 7.6	16.5 ± 7.5	ns	ns	****	****
Food (g)	2.3 ± 0.7	2.1 ± 0.7	4.6 ± 1.1	4.3 ± 0.5	ns	ns	****	****
20 weeks								
Urine (ml)	0.7 ± 0.4	0.8 ± 0.5	22.7 ± 4.6	18.2 ± 8.0	ns	*	****	****
H_2O (ml)	4.1 ± 1.0	4.4 ± 1.8	25.7 ± 5.0	21.8 ± 8.0	ns	ns	****	****
Food (g)	2.3 ± 0.6	2.1 ± 0.6	5.2 ± 0.5	4.7 ± 0.8	ns	ns	****	****

Data are mean ± SD, n=9–10 per group. Two-way ANOVA was performed comparing factor variables, with Bonferroni post hoc test. CIT, citrate control (non-diabetic); STZ, streptozotocin-induced diabetes. *P<0.05, ****P<0.0001, ns = not significant P>0.05

membranes, before being blocked for 1 h in 5% skim milk in Tris buffered saline with 0.1% Tween-20 (TBS-T). Membranes were incubated overnight with gentle agitation at 4°C with 6.2 μg/μl total OXPHOS rodent antibody (ab110413, Abcam, Melbourne, Australia), before being incubated at room temperature in an IRDye® 800CW goat anti-mouse IgG secondary antibody (LI-COR Biosciences, Lincoln, NE, U.S.A.) for 90 mins. Membranes were visualised using an Odyssey Infra-REd imaginf platform (LI-COR Biosciences, Lincoln, NE, U.S.A.) and were quantified using Image Studio Lite v5.2. An internal standard was loaded on each gel to account for gel-to-gel variability. Whole lane stain-free quantification (Bio-Rad Chemi-Doc imaging system, and Bio-Rad Image Lab 5.2.1 imaging software; Bio-Rad laboratories, Gladesville, NSW, Australia) was used to normalise total protein per well, and qualitatively verify correct loading and equal transfer between lanes. Additionally, an internal control sample was applied across all gels and used to normalise data between gels.

Statistics

All statistical computations were performed using GraphPad Prism version 7.0 (GraphPad Software, San Diego, California, U.S.A.). Values of experimental groups are given as mean, with error bars showing SD, unless otherwise stated. Outliers were only excluded where a valid biological or technical issue indicated exclusion. Two-way ANOVA was performed with unweighted means. Bonferroni post-hoc test was used to determine statistical significance and correct for multiple comparisons between each factor. P<0.05 was considered to be statistically significant. Additionally, significance in graphs is indicated as: *P<0.05, **P<0.01, ***P<0.001, ****P<0.0001, where required a two-way ANOVA with repeated measures was performed on data representing different time points with $^{\S}P$<0.05.

Results

CypD deletion does not protect against diabetes-induced renal injury

As expected, hyperglycaemia and decreased body weight occurred with diabetes (Table 1). Additionally, diabetes-associated renal hypertrophy developed, shown as an increase in total kidney weight and kidney to body weight ratio. Diabetic mice had increased daily water and food consumption and developed polyuria. Genetic deletion of CypD did not alter fasting blood glucose concentrations in non-diabetic mice nor in the setting of diabetes (Table 1). There was a significant decrease in body weight in non-diabetic *Ppif*$^{-/-}$ mice. CypD (*Ppif*) deletion also decreased polyuria at both 12 and 20 weeks of diabetes. Water consumption and food intake remained similar between diabetic *Ppif*$^{WT/WT}$ and *Ppif*$^{-/-}$ groups during the 24 h period.

Clinical Science (2020) **134** 239–259
https://doi.org/10.1042/CS20190787

Table 2 Phenotypic and metabolic characteristics of db/m and db/db mice

	db/m vehicle	db/m Alisporivir	db/db vehicle	db/db Alisporivir	Two-way ANOVA comparison	
	Mean ± SD	Mean ± SD	Mean ± SD	Mean ± SD	Vehicle db/m vs db/db	db/db vehicle vs Alisporivir
Cull weight (g)	29.1 ±2.3	29.7 ±3.4	38.2 ±8.3	34.4 ±7.3	***	ns
Glucose† (mmol)	10.3 ±1.4	10.1 ±1.8	28.6 ±12.1	25.0 ±13.4	****	ns
HbA_{1C}‡ (%)	4.7 ±0.1	4.6 ±0.6	12.4 ±1.6	11.7 ±2.6	****	ns
EchoMRI						
Fat (g)	5.1 ±1.7	4.4 ±1.3	18.3 ±6.00	14.3 ±6.5	****	ns
Lean (g)	23.5 ±1.9	24.0 ±3.2	21.7 ±2.1	21.1 ±2.1	ns	ns
Total (g)	28.7 ±2.3	28.3 ±3.1	40.0 ±6.6	35.5 ±6.2	****	ns
Total kidney weight (g)	0.36 ±0.1	0.40 ±0.1	0.46 ±0.1	0.48 ±0.1	*	ns

Two-way ANOVA performed, with Bonferroni post hoc test comparing each factor variable. *P<0.5, ***P<0.001, ****P<0.0001; ns is P>0.05; n=11–15.
†Fasting Spot glucose test at endpoint.
‡HbA_{1C}, for glycated haemoglobin.

Albuminuria (urinary albumin excretion) (Figure 1A) and urinary albumin to creatinine ratio were significantly increased in all STZ treated mice (Figure 1B). In addition, urinary excretion of the tubular damage-associated marker KIM-1 was increased in diabetic animals but was not different $Ppif^{-/-}$ mice (Figure 1C). Plasma cystatin C, a surrogate marker of glomerular filtration rate, was reduced in the STZ model indicative of hyperfiltration (Figure 1D). Genetic deletion of CypD in the setting of diabetes led to a prevention of hyperfiltration, as shown by no decrease in plasma cystatin c in the $Ppif^{-/-}$ STZ group. Conversely, deletion of CypD decreased GFR, measured as elevated cystatin C in both control and diabetic $Ppif^{-/-}$ mice.

GSI was assessed in PAS-stained glomeruli (Figure 1E) and mean histology scores were significantly increased in all STZ treated animals compared with controls. $Ppif^{-/-}$ STZ mice exhibited higher GSI histology scores compared with wild-type STZ indicating that the absence of CypD exacerbated glomerular injury in a diabetic setting. This was reiterated by an increase in diabetes-associated glomerular collagen IV deposition (Figure 1F) in the $Ppif^{-/-}$ STZ mice. Thus, loss of CypD via deletion of the Ppif gene exacerbated glomerular structural injury in our model of DKD.

Deletion of cyclophilin D modulates mitochondrial ATP synthase F1-α

To confirm that the renal phenotype was indeed related to a loss of CypD, deletion of the gene encoding for CypD, *Ppif* was confirmed by quantitative reverse transcription-polymerase chain reaction (RT-qPCR). No expression of the *Ppif* gene was detected in the $Ppif^{-/-}$ mice (Figure 2A). No change in *Ppif* expression was observed between WT control and STZ diabetic animals. To ascertain that deletion of *Ppif* did functionally reduce mitochondrial swelling, a calcium overload assay was performed in isolated mitochondria from $Ppif^{WT/WT}$ and $Ppif^{-/-}$ animals to induce mPTP opening (Figure 2B). Diabetic $Ppif^{-/-}$ mice had decreased calcium-induced swelling as compared with WT diabetic mice. Since CypD binds to F_1/F_0 of the ATP synthase complex, we tested the gene expression of the *F1-α* component. $Ppif^{-/-}$ mice had a marked down-regulation of this gene, in addition to a 50% reduction seen in the $Ppif^{WT/WT}$ STZ treated mice (Figure 2C). Another mitochondrial gene, cytochrome *c*, was also down-regulated by both STZ treatment and in $Ppif^{-/-}$ mice (Figure 2D). Gene expression of the fibrosis-associated fibronectin protein (Figure 2E) was increased 5-fold in $Ppif^{WT/WT}$ STZ mice. Genetic deletion of $Ppif^{-/-}$ in diabetic mice decreased the fibronectin gene expression similar to control levels. Collagen IV gene expression however was not increased with diabetes, and was down-regulated in $Ppif^{-/-}$ mice (Figure 2F).

Pharmacological inhibition of cyclophilin D with 5 mg/kg Alisporivir did not alter blood glucose control or body composition of db/db mice

Db/db mice had increased body weight compared with *db/m* mice consistently over the course of the study (Figure 3A). A decline in body weight towards end point of the study was noted in some diabetic animals, which is considered to reflect the development of pancreatic β-cell failure. Alisporivir did not reduce diabetes-associated hyperglycaemia nor glycated haemoglobin levels in *db/db* diabetic mice (Table 2). Assessment of body composition by EchoMRI (Table 2) showed that the increase in body mass was attributable to a two-fold increase in fat mass in all *db/db* mice irrespective of therapy (Figure 3B). Endpoint body mass of *db/db* mice also did not differ between vehicle and drug treated animals at week 16 of treatment (Figure 3C). As expected, diabetic *db/db* animals developed renal hypertrophy

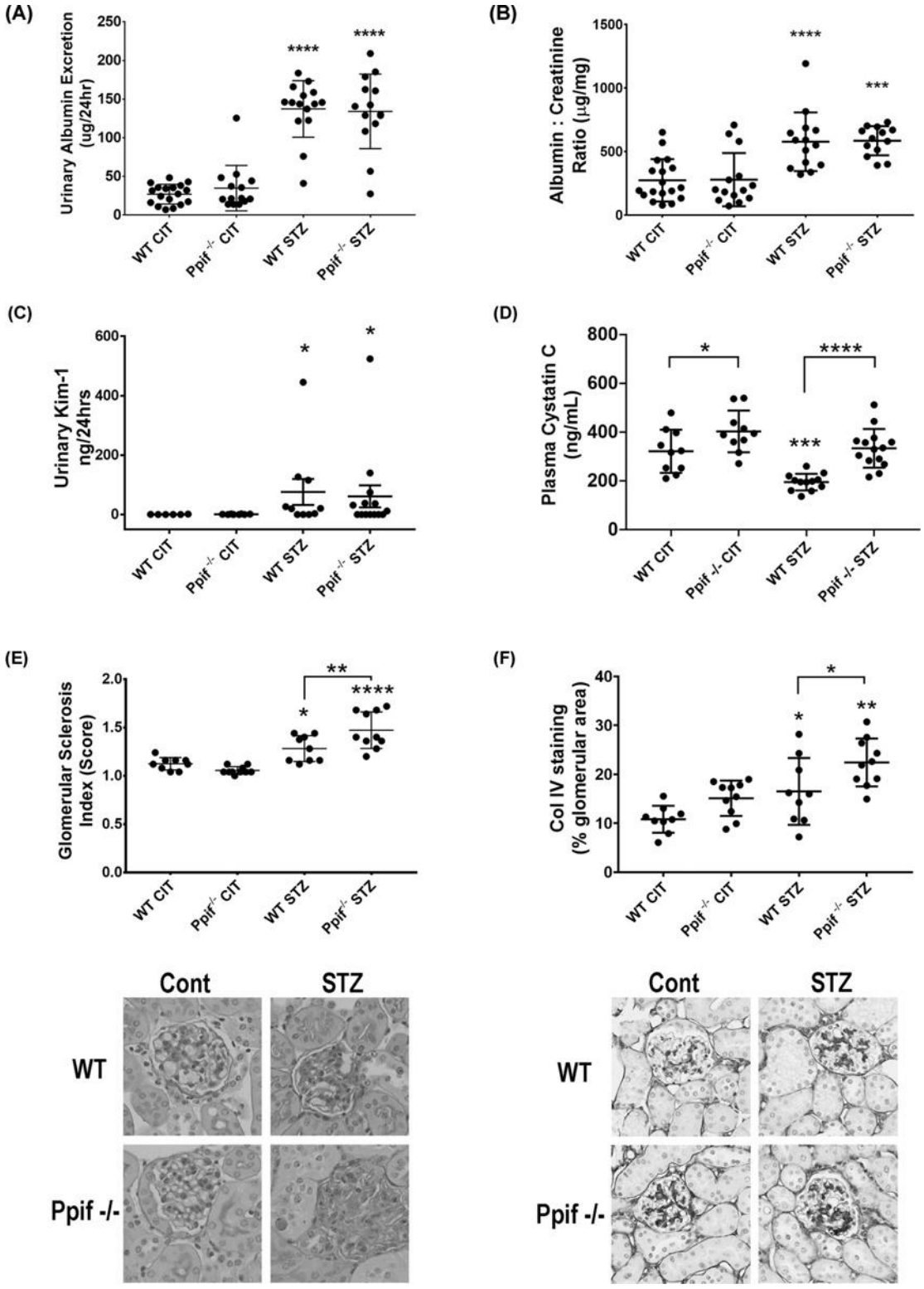

Figure 1. Cyclophilin D deletion does not protect against diabetes-induced renal injury

(**A**) Urinary albumin excretion; (**B**) urinary albumin to creatinine ratio, mean ± SD shown; (**C**) urinary excretion of KIM-1; (**D**) plasma cystatin C; (**E**) GSI, with representative photomicrographs of PAS-stained renal cortex, ×400 magnification; (**F**) collagen IV deposition, with representative photomicrographs of collagen IV immunohistochemistry in renal cortex, ×400 magnification. Data are mean ± SEM unless otherwise stated, n=9–14 mice per group. Two-way ANOVA with Bonferroni post hoc test was performed where *P<0.05, **P<0.01, ***P<0.001, ****P<0.0001.

Clinical Science (2020) **134** 239–259
https://doi.org/10.1042/CS20190787

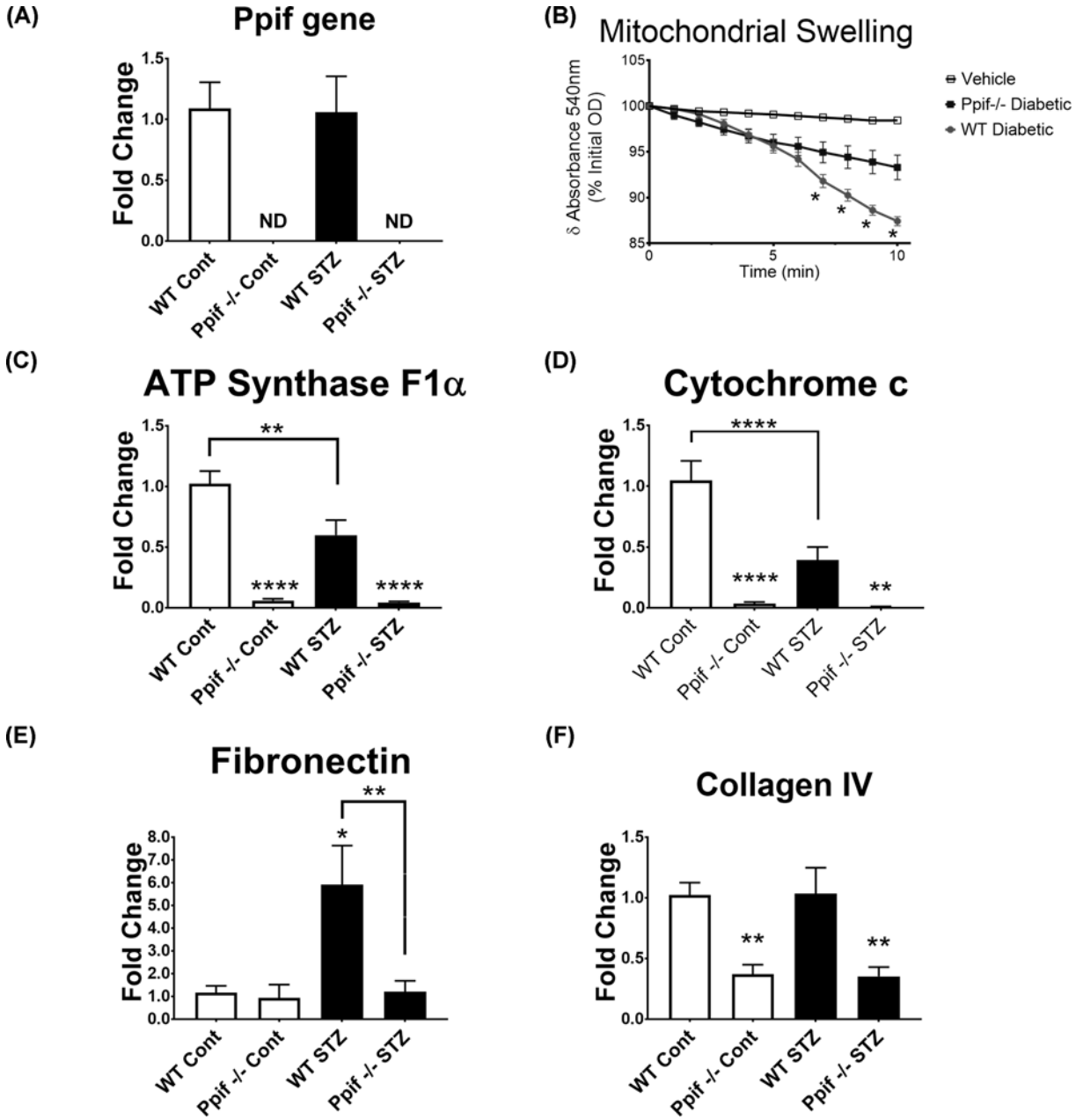

Figure 2. Deletion of cyclophilin D (*Ppif*) inhibits mitochondrial swelling and alters gene expression profiles

(**A**) Deletion of Ppif gene confirmed by RTqPCR; (**B**) mitochondrial swelling by calcium challenge; (**C**) qPCR for ATP synthase F1α gene; (**D**) RTqPCR for cytochrome *c* gene; (**E**) RTqPCR for fibronectin gene; (**F**) RTqPCR for collagen IV gene. Data are mean $\pm$ SEM, n=9–14 mice per group. Two-way ANOVA with Bonferroni post hoc test was performed with $^{*}P<0.05$, $^{**}P<0.01$, $^{****}P<0.0001$.

with increased total kidney weight (Table 2). confirmed by an increase in the kidney to body weight ratio (Figure 3D) which was not affected by Alisporivir.

Alisporivir does not attenuate renal pathology in db/db mice

Plasma cystatin C as a marker of glomerular filtration rate, was unchanged for all *db/db* and *db/m* mice in the present study (midpoint—Figure 3E, endpoint—Figure 3F). Both urinary albumin excretion rate (midpoint—Figure 4A, endpoint—Figure 4B) and albumin to creatinine ratios (Figure 4C) were increased in all *db/db* animals consistent with DKD progression and was not attenuated by Alisporivir. Urinary KIM-1 was also increased in both *db/db* groups and unaffected by Alisporivir (Figure 4D). *Db/db* mice had increased Glomerular Sclerosis Index compared

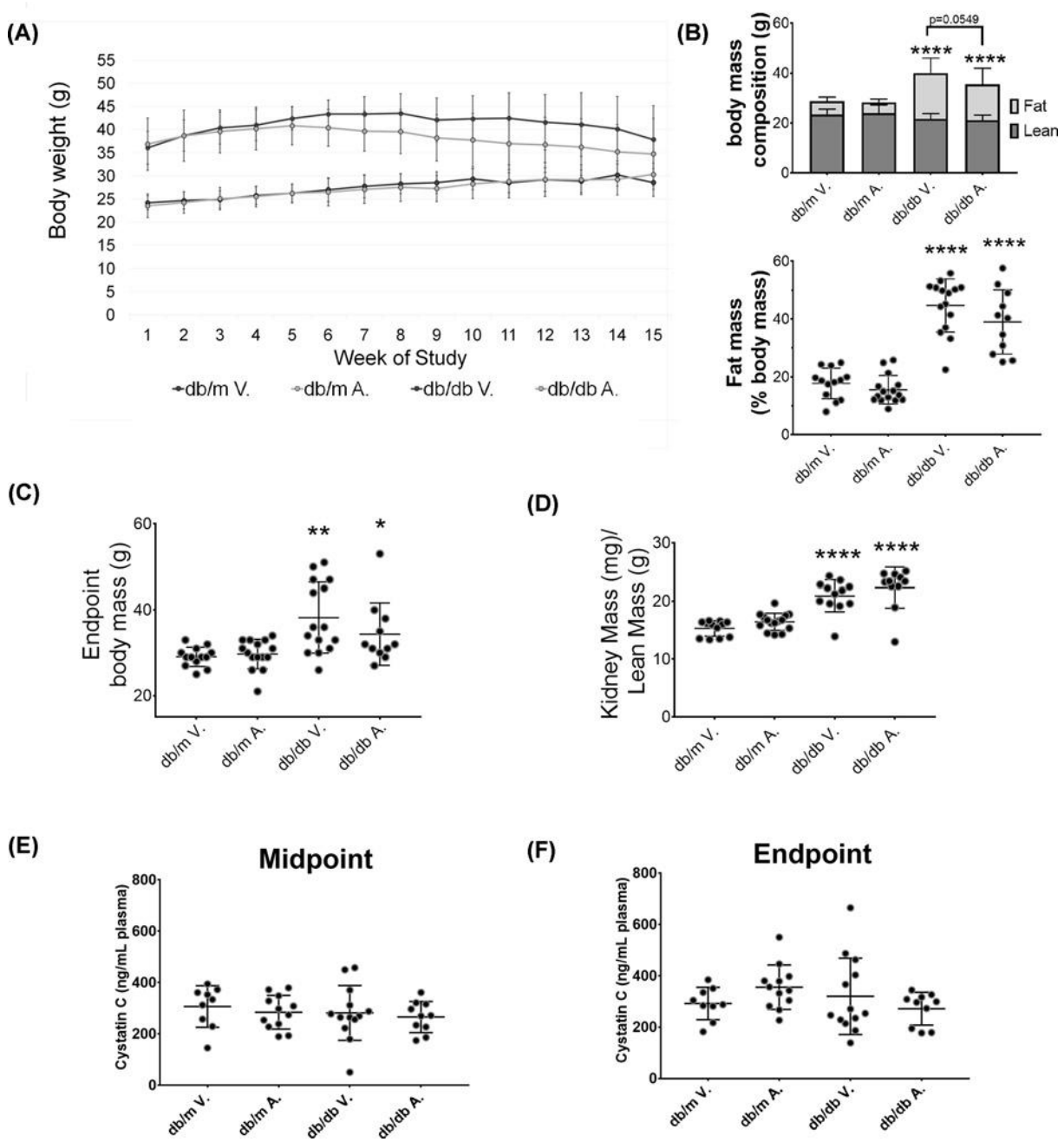

Figure 3. *Db/db* mice develop obesity and hyperglycaemia with associated renal hypertrophy and Albuminuria, which was unchanged with Alisporivir

(**A**) Average body weights during study; (**B**) body mass index as assessed by EchoMRI showing average lean and fat mass (top) and individual % body fat (bottom). (**C**) Final body mass at 16 weeks of study; (**D**) kidney weight to lean body mass; plasma cystatin C measured at midpoint (**E**) and endpoint (**F**). Data are mean ± SD, Two-way ANOVA with Bonferroni post hoc test was performed with $^{*}P<0.05$, $^{**}P<0.01$, $^{****}P<0.0001$. n=9–15 mice per group.

to *db/m* controls, however, Alisporivir had no impact on glomerular injury in *db/db* mice (Figure 4E). No increase in glomerular *Col IV* deposition between vehicle *db/m* and *db/db was seen in the present study* (Figure 4F), however, *Db/m* animals receiving Alisporivir had decreased *Col IV* deposition compared with vehicle controls. A comparison of these results and those of the *Ppif* study for the effects of diabetes and targeting *Ppif* (CypD) is provided in Table 3.

Clinical Science (2020) **134** 239–259
https://doi.org/10.1042/CS20190787

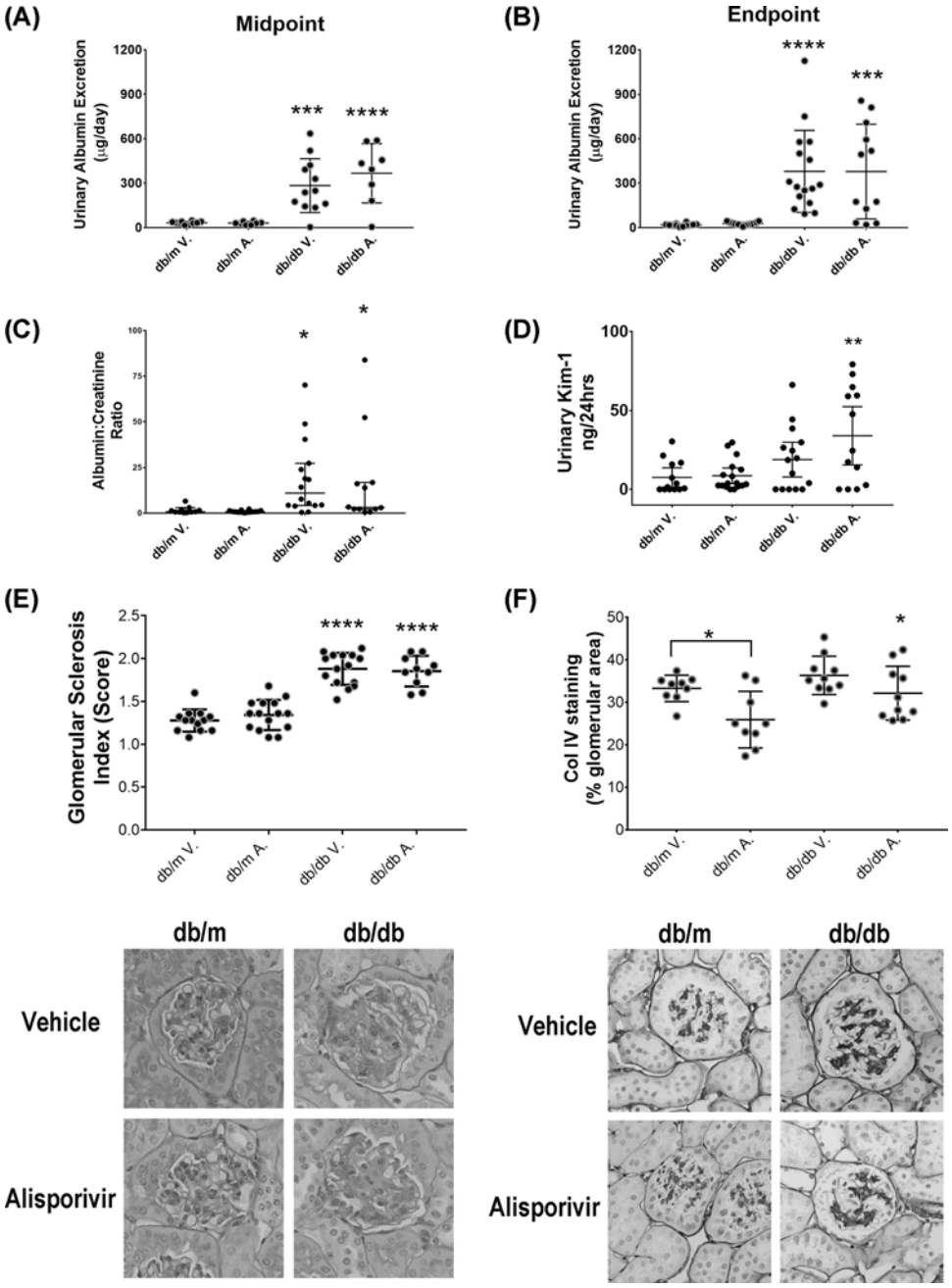

Figure 4. Treatment with Alisporivir does not alleviate markers of diabetes-associated renal injury

Albuminuria measured as urinary albumin excretion per day for midpoint (**A**) and endpoint (**B**); (**C**) albumin to creatinine ratio at endpoint; (**D**) detection of Kim-1 in 24 h urine by ELISA, mean with 95% CI shown; (**E**) GSI assessed in 3 mm PAS-stained sections of renal cortex, with representative photomicrographs at ×400 magnification; (**F**) glomerular collagen IV deposition assessed by immunohistochemistry in 4 μm renal cortical sections, with representative photomicrographs, ×400 magnification. Data are mean ± SD. Two-way ANOVA with Bonferroni post hoc test was performed with $^{*}P<0.05$, $^{**}P<0.01$, $^{***}P<0.001$, $^{****}P<0.0001$. n=9–15 mice per group.

Alisporivir does not improve sedentary behaviour or whole-body energy calorimetry in db/db mice

Daily physical activity was assessed by 'beam breaks' in X+Y+Z directions in the CLAMS system over 24 h. These data are shown as discrete measurements across the light (inactive/sleep) and dark (active) cycles (Figure 5A) and

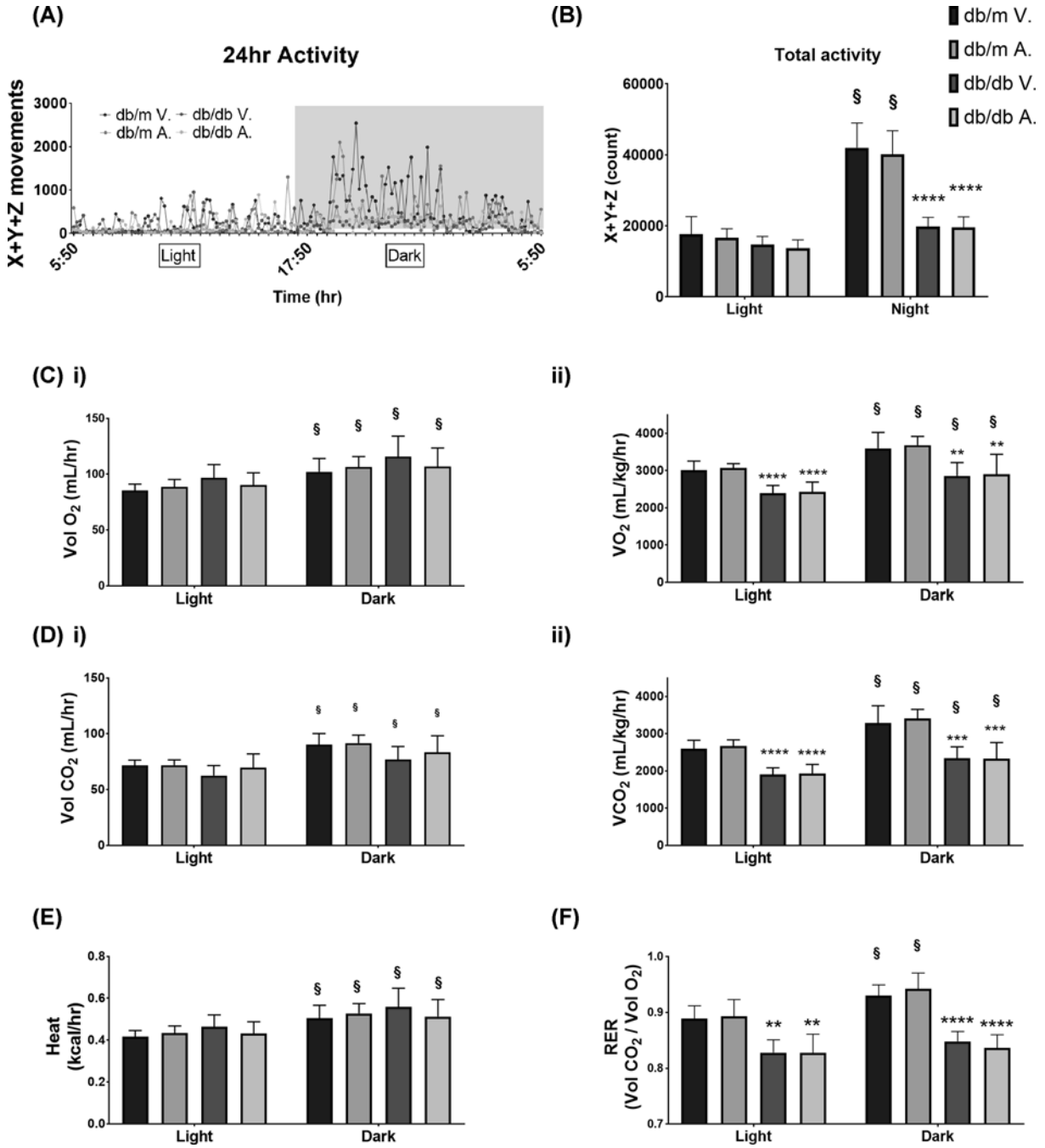

Figure 5. Comprehensive Laboratory Animal Monitoring System revealed Alisporivir has no effect on activity or respiration in db/db mice

(**A**) Representative graphs (n=1 per group) for total movements assessed by beam breaks in X+Y+Z planes over 24 h; (**B**) mean and 95% CI for Sum of all movements during light (sleep) and dark (active) periods; (**C**) oxygen consumption: (i) ml/h, (ii) ml/kg/h; (**D**) carbon dioxide production: (i) ml/h, (ii) ml/kg/h; (**E**) heat production; (**F**) RER Vol CO_2/Vol O_2. Data are mean ± 95% CI. n=8–10 mice per group. Two-way ANOVA with Bonferroni post hoc test comparing *db/m* vs *db/db.* $^{**}P<0.01$, $^{***}P<0.001$, $^{****}P<0.0001$. No difference between vehicle (V.) and Alisporivir (A.) was found for any parameter. Two-way ANOVA with repeated measures was performed comparing light and dark time points with Bonferroni post hoc test where § shows $P<0.05$.

Clinical Science (2020) **134** 239–259
https://doi.org/10.1042/CS20190787

Table 3 Summary of key results

	STZ model of T1DM	Genetic *Ppif* deletion	Interaction†	*db/db* model of T2DM	Alisporivir (5 mg/kg/day)	Interaction‡
Renal hypertrophy	Present	No change	No change	Present	No change	No change
Structural glomerular injury	Moderate	Mild	Worsened	Moderate	No change, or mild reduction	No change
Glomerular filtration estimate	Lowered	Increased	Intermediate	No change	No change	No change
Urinary damage markers	Increased	No change	No change	Increased	No change	No change

Comparison of key pathological changes observed in both mouse models. The impact of diabetes and targeting CypD (*Ppif*) are summarised in comparison to control mice. The interactive effects between diabetes and reduction in CypD represent the changes observed in: † the $Ppif^{-/-}$ STZ treated group; and ‡ the db/db mice treated with Alisporivir. Abbreviations: T1DM, Type 1 diabetes; T2DM, Type 2 diabetes.

also as cumulative totals (Figure 5B). *Db/m* mice performed double the physical activity during the dark cycle (active period) compared to the light cycle. *Db/db* animals remained sedentary during dark cycle, with a significant reduction in physical activity compared to *db/m* controls.

Respiration was analysed via changes in oxygen consumption and carbon dioxide production. All individual mice had increased ($^{\S}P<0.05$) respiration during the dark period compared to the light for both O_2 (Figure 5C) and CO_2 data (Figure 5D). No significant differences were evident between *db/db* versus *db/m* mice for either oxygen (Figure 5Ci) or carbon dioxide respiration (Figure 6Ci) measured in ml/h. There were, however, slight trends toward an increase in O_2 (Figure 5Ci) and a decrease in CO_2 (Figure 5Di) for *db/db* mice on vehicle but not Alisporivir. When normalised to body weight (ml/kg/h) this trend disappeared and both *db/db* groups were significantly decreased compared with their *db/m* controls (Figures 5Cii and 6Cii). Energy expenditure (heat production) was unchanged between all groups (Figure 5E) respiratory exchange ratio (RER), which is reflective of metabolic substrate preference, was calculated from the ratio of Volume of CO_2 to Volume O_2. Once again, values were higher in *db/m* mice during the dark cycle compared to the light, indicating increased carbohydrate metabolism during active hours. Interestingly, however, no such difference was observed in *db/db mice*. Additionally, the slight trends in O_2 and CO_2 respiration observed in Figure 5C,D synergistically resulted in a statistically significant decrease in RER in *db/db* animals with no change with Alisporivir (Figure 5F). This decrease in RER is reflective of a preference for fat metabolism in *db/db* mice. Overall, pharmacological inhibition of CypD had little effect on any parameter observed with the CLAMS system.

Renal cortical mitochondrial oxygen consumption rate was increased in db/db mice

Next, markers of mitochondrial respiratory function and mPTP were assessed. Citrate synthase activity, an overall marker of mitochondrial quality, was determined and revealed no significant difference in enzyme activity between groups per μg of isolated mitochondria (Figure 6A) indicating that any differences observed in mitochondrial activity are attributable to functional measures rather than changes to overall mitochondria quality. The mitochondrial swelling response induced by calcium challenge showed no statistically significant differences for the rate of Δabsorbance at 540 nm (Figure 6B). The isolated mitochondrial preparations were also pretreated with the mPT inhibitor CsA, prior to receiving the calcium challenge. Interestingly, this pretreatment differentially affected the total duration of swelling inhibition between *db/m* and *db/db* mice, whereby mitochondria from the *db/db* mice underwent a rapid drop in absorbance (i.e. no swelling inhibition). Treatment with Alisporivir partially restored CsA inhibition of the mPTP in *db/db* mice, however, the mean group average was not significantly different from the vehicle *db/db* mice.

To assess mitochondrial respiration in the kidney, a mitochondrial stress test was performed in the Seahorse Bioanalyser using glutamate/malate to test complex I-linked respiration in isolated mitochondria (Figure 6C). A significant increase in OCR following ATP and FCCP injections was observed for vehicle treated *db/db* mice, but this was lessened in Alisporivir treated *db/db* mice. RCR (State 3/State 4o) and ATP-linked respiration of isolated kidney mitochondria were increased in vehicle *db/db* mice compared with *db/m* controls (Figure 6D). Although there was a trend towards a reduction in complex I-stimulated respiration in Alisporivir treated *db/db* mice this was not statistically significant. No differences in proton leak or FCCP stimulated respiration were observed.

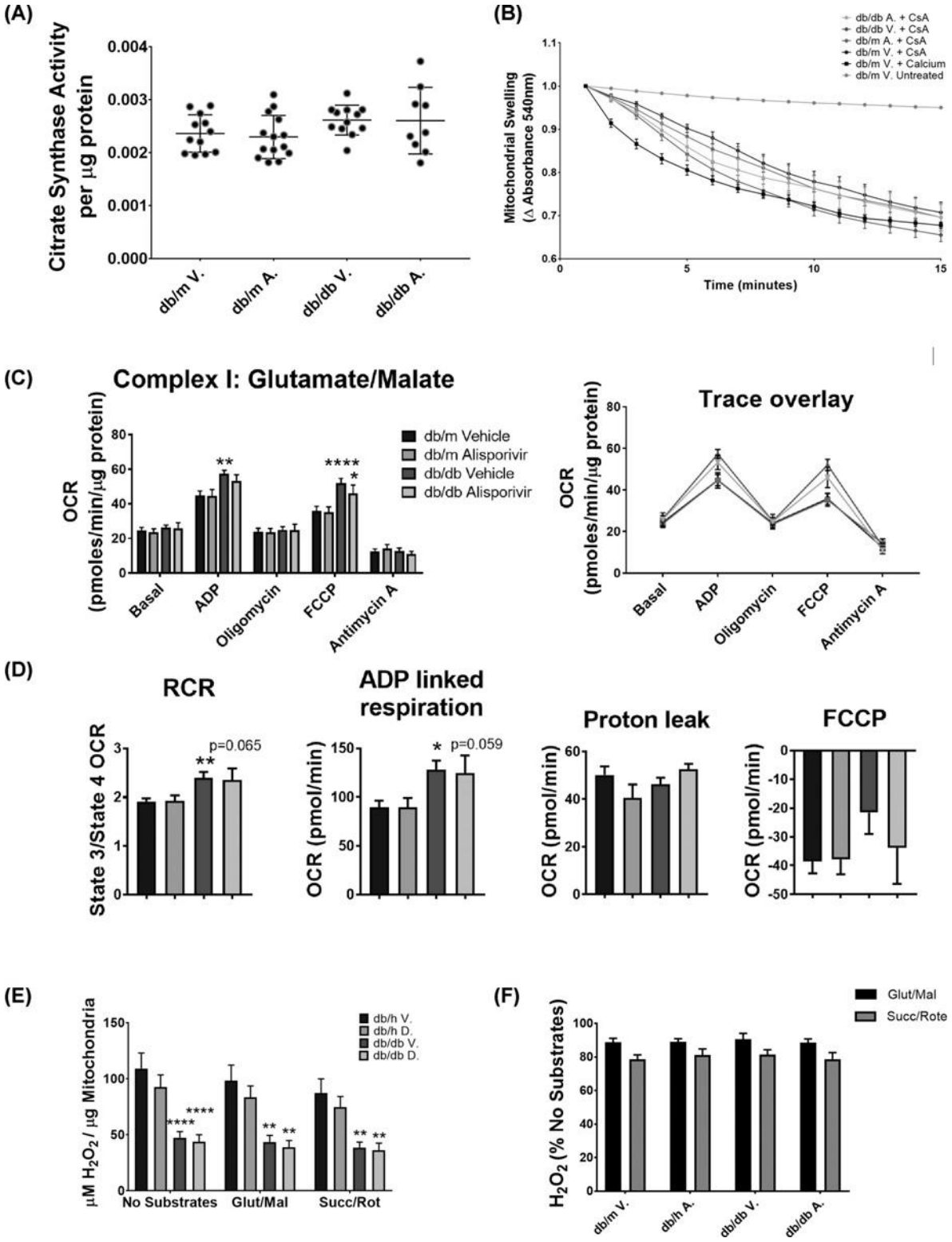

Figure 6. *Db/db* mice exhibit changes in mitochondrial function with minor modulation by Alisporivir

(**A**) Citrate synthase activity in isolated renal cortex mitochondria mean ± SD; (**B**) calcium induced mitochondrial swelling; (**C**) (left) mitochondrial stress test with glutamate + malate-stimulated complex I respiration, (right) respiration trace overlay; (**D**) calculated respiratory control ratio (RCR), ADP-linked respiration, proton leak and FCCP-stimulated OCR; (**E**) H_2O_2 production in isolated mitochondria; (**F**) H_2O_2 production normalised to 'no substrate' control. Data are mean ± SEM unless otherwise stated. Two-way ANOVA with Bonferroni post hoc test was performed with $^*P<0.05$, $^{**}P<0.01$, $^{****}P<0.0001$. n=9–15 mice per group.

Clinical Science (2020) **134** 239–259
https://doi.org/10.1042/CS20190787

Hydrogen peroxide species generation was decreased in db/db mice

H_2O_2 generated by isolated mitochondria, and measured by Amplex red fluorescence intensity was halved in the *db/db* mice compared to *db/m* controls with no difference between vehicle and Alisporivir treated *db/db* mice (Figure 6E). Percentage H_2O_2 generation with substrates was normalised to no substrates, and was found to be unchanged between groups (Figure 6F), therefore indicating that the decrease in total H_2O_2 was not substrate-dependent.

Db/db mice had altered gene expression profiles for several mitochondrial and cell death genes

Renal cortical gene expression of several cell death and mitochondrial-associated proteins were assessed by RT-qPCR in the *db/db* model to determine the effect of diabetes and treatment with Alisporivir on these mitochondrial centred pathways (Figure 7A). Treatment with the *CypD* inhibitor Alisporivir did not alter the gene expression of its associated gene (*Ppif*) in *db/m* mice, however, in the context of diabetes *Ppif* expression was significantly increased. Interestingly there was an up-regulation of *Cytc* observed in the *db/m* mice treated with Alisporivir, however no change was present with diabetes in the *db/db* mice in contrast with the STZ model described above. Multiple other genes in both cell death and mitochondrial function were also assessed. Firstly, inflammation-associated *TGF-β* and macrophage-associated *F4/80* gene expressions were unchanged. Secondly, expression of several cell death activator caspases were also unchanged, although there was a significant increase in the inflammation-associated caspase 12 (Human equivalent of CASP 4) in vehicle treated *db/db* diabetic mice only. Additionally, some fibrosis related genes, including collagen I and fibronectin, were up-regulated in vehicle *db/db* mice and partially attenuated in those treated with Alisporivir. Smooth muscle actin-alpha (α-SMA) and connective tissue growth factor (CTGF) did not change with diabetes.

Changes in genes associated with mitochondrial dynamics were minimal with the exception of a modest increase in *Mief1* expression in *db/db* mice treated with vehicle which was not seen with Alisporivir. Finally, a fold change increase in the mitochondrial uncoupling protein-2 (*Ucp-2)* gene expression was statistically significant for *db/db* mice treated with and without Alisporivir.

Mitochondrial content was increased in db/db mice with no relative change in electron transport system complexes

Mitochondrial electron transport system (ETS) complex protein expression was not different between *db/m* and *db/db* mice with no change in complex I to V protein expression detected by Western blot (Figure 7B).

Transmission electron microscopy of dissected renal cortices of *db/m* and *db/db* mice at endpoint showed that mitochondrial dynamics were not altered in *db/db* mice compared with *db/m* mice as assessed by the mitochondrial shape descriptors for Form Factor (Supplementary Figure S1A). However, *db/db* mice exhibited an increase in 2D volume of mitochondria from approximately 30–35%/μm^2 of cytosolic area in the proximal tubule cells (Figure 7C). This may be reflected in the shift in the frequency distribution of mitochondrial area (Supplementary Figure S1B).

Discussion

The mPTP has long been considered to play an important role in mediating the demise of mitochondria in response to overwhelming stress. Although the exact mechanism of pore activation remains under investigation, the protein CypD continues to be regarded as an important regulator of mitochondrial swelling and function [10,14,27–29]. In the present study we demonstrated that global deletion of the CypD gene, *Ppif,* in C57BL6 mice was not associated with the development of any overt systemic pathology. This is consistent with other reports using $Ppif^{-/-}$ mice where phenotypes were limited to minor metabolic alterations, for example calcium handling and body fat metabolism [30–32]. Indeed, our study showed some significant differences between $Ppif^{-/-}$ and $Ppif^{WT/WT}$ in non-diabetic mice with changes limited to slightly reduced body weight and lower collagen IV deposition. The increase in cystatin C in $Ppif^{-/-}$ mice indicated that deletion of CypD was protective against the development of diabetes-associated hyperfiltration. However, this elevated cystatin C could also be interpreted as a decline kidney function, even in non-diabetic mice, considering that the albumin to creatinine ratio was unchanged between $Ppif^{WT/WT}$ and $Ppif^{-/-}$. Additionally, lack of CypD was associated with an increase in the structural damage in the kidney in our model of STZ induced DKD. This increase in renal damage, following deletion of a key mPTP sensitising protein, provides supporting evidence for the complex biological role of CypD beyond providing a failsafe to initiating mitochondrial cell death [33].

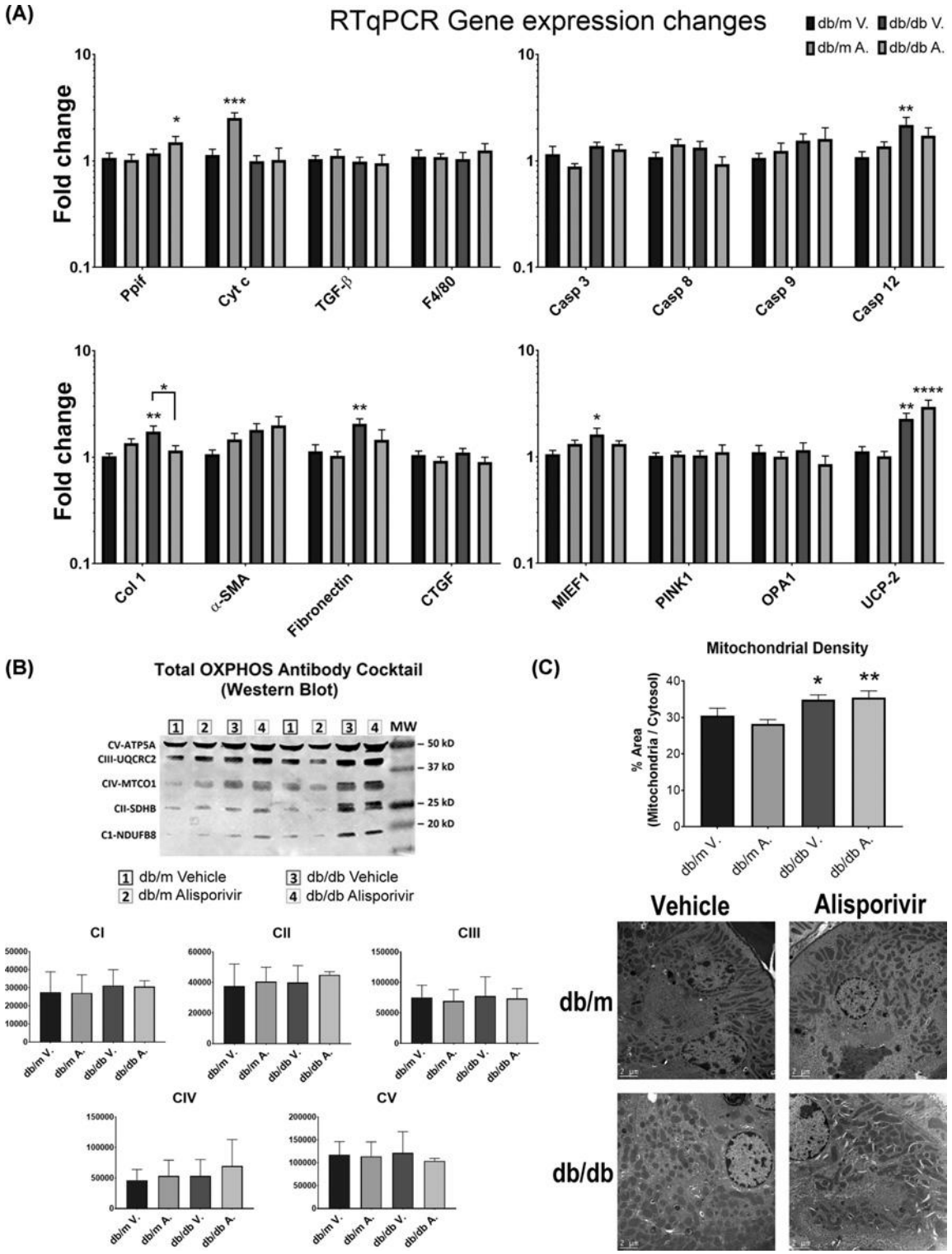

Figure 7. Alisporivir treatment induced minor changes in diabetes-induced mitochondrial gene expression but did not alter ETS protein expression, nor increased 2D volume

(**A**) RTqPCR gene expression changes in whole renal cortex, relative fold change compared with db/m vehicle (V.). Mean ± SEM, n=9–14 per group. (**B**) ETS complexes, protein expression assessed by Western blot. Representative image with n=2 per gel, per experimental group. Graphs show mean ± SD of n=6 total. (**C**) Transmission electron microscopy assessment of 2D mitochondrial volume in renal PTECs. Graph shows mean ± SEM for n=3 per group with representative electron micrographs (17.44 × 17.44 μm). Two-way ANOVA with Bonferroni post hoc test was performed with *P<0.05, **P<0.01, ***P<0.001, ****P<0.0001.

Clinical Science (2020) **134** 239–259
https://doi.org/10.1042/CS20190787

Data from our study also revealed that CypD (*Ppif*) deletion was associated with a decrease in the relative fold change expression of multiple genes tested by qPCR (plus additional genes not presented) compared to the WT controls. This reduction in gene expression may be explained by the ability of cyclophilins to regulate gene expression processes [34]. Although the qPCR data for fibrosis genes appear to suggest an improvement in $Ppif^{-/-}$ STZ diabetic mice, the histology data may suggest that remodelling has already occurred.

It is generally well established that mPTP activity affects multiple organ systems, including liver function and skeletal muscle [30,35–37]. This is in part due to its role in regulating crucial mitochondrial functions and temporary mPTP depolarisation for physiological purposes [9,33,35]. Further, CypD has been shown to negatively regulate F_1/F_0 ATP synthase activity, by binding to the Oligomycin-Sensitivity Conferring Protein (OSCP) (which links the F1 portion with the lateral stalk) thereby limiting ATP coupling and energy production [38–40]. ATP synthase remains a reasonable candidate for the main component of the mPTP channel, making this interaction with CypD imperative [41,42]. The requirement of these processes in the diabetic kidney is highlighted by the apparent increase in glomerular structural damage observed in the $Ppif^{-/-}$ mice in our study. Interestingly, the mechanism for why CypD deletion attenuates other diabetes-related complications, such as pancreatic function and cognitive decline, has been demonstrated previously to be modulated by inhibiting β-oxidation and increasing substrate metabolism through glycolysis [36,43]. However, metabolic alterations of CypD deletion have demonstrated variability in different organs for different genetic models, e.g. liver, skeletal muscle [34–36]. In the kidney, CypD has also been previously demonstrated to be a key regulator of cellular metabolism with deletion of the *Ppif* gene (CypD) leading to an increase in glycolysis at the expense of fatty acid oxidation (FAO) [44]. These changes in glycolytic metabolism are pertinent in the renal cortex where β-oxidation provides a crucial fuel source to PTECs and this switch in fuel generation is likely to be detrimental, as reduced capacity of FAO has been associated with increased renal fibrosis as a consequence of acute stress [45]. Further, disruption to FAO pathways, as observed in patients with CKD, is associated with renal fibrosis [46]. Diabetes is also independently associated with changes in renal cellular metabolism including reduced FAO alongside a total increase in lipid accumulation [47]. The combined effect of both loss of CypD and the chronic metabolic stress induced by diabetes could be expected to lead to an increase in renal fibrosis. Indeed, loss of CypD has been previously hypothesised to prime PTECs to stress [44]. Thus, a switch to glycolysis in the diabetic kidney, at the expense of β-oxidation, could explain why renal injury is recapitulated in our model.

Although complete loss of CypD, via *Ppif* deletion, was associated with negative consequences with respect to our STZ model of DKD, pharmacological blockade of CypD was still a pertinent option to explore as partial inhibition may allow maintenance of some physiological functions. The drug Alisporivir is a cyclosporine analogue which has demonstrated ability to bind CypD and prevent its participation in mPT pore formation, without conferring the immunosuppressive effects of earlier cyclosporines [48–50]. Although Alisporivir was initially developed by Debiopharm as an antiviral drug to target HIV and hepatitis C infection, it has demonstrated efficacy in improving mitochondrial function and associated pathological outcomes in a range of acute disease settings by preventing cell death and rescuing mitochondrial function [51–54]. The drug profile includes a demonstrated ability to reduce lesion size following cardiac infarction, and potentially as a prophylactic measure to protect kidney cells from renotoxic substances used during cardiac surgery [55,56]. This is a promising result since a wide range of commonly used drugs induce renal toxicity and require monitoring of kidney function. Some prominent clinical studies, however, question the efficacy of acute CypD targeted therapy (cyclosporines) in preventing cardiac pathologies [57,58]. Nonetheless, research into Alisporivir's efficacy in treating chronic diseases is now being considered, with promising studies in mouse models of muscular dystrophy revealing the potential for a long-term therapeutic strategy to rescue mitochondrial function in certain chronic diseases [59,60].

Here, we reveal that Alisporivir at a dose of 5 mg/kg/day did not protect the kidney from the development of clinical nephropathy markers in DKD. Indeed, we may consider that higher therapeutic doses could have increased efficacy, however in our study, a dose of 10 mg/kg was associated with an attenuation of hyperglycaemia in *db/db* mice to *db/m* control levels (data not shown). This effect is a confounding variable as high blood glucose is a well-established risk factor for diabetic complications. Strict blood glucose control is the gold standard for clinical diabetes care; thus, any renal protection mechanism of the drug alone at such glucose lowering doses cannot be independently assessed. This result may be worth exploring in future studies to further elucidate alterations in glucose metabolism and glycaemic control with such an agent. Our data revealed that treatment with 5 mg/kg/day Alisporivir was not associated with an exacerbation of renal damage, in either control or diabetic animals. This is important as cyclosporines can induce significant nephrotoxicity in a dose dependent manner; mediated through autophagy, oxidative stress and ER stress [61–63]. Indeed, dose management concerns are often raised in patients prescribed analogues for immunosuppressant purposes [64–65]. Currently there are limited data available on the pharmacodynamics of Alisporivir in renal tissues.

Our data indicates that 5 mg/kg/day Alisporivir was well tolerated in male *db/db* mice, providing evidence that this modified analogue may have reduced renal toxicity over traditional cyclosporine analogues.

Interestingly, although Alisporivir had minimal effect on renal injury, there were a number of changes observed in the renal cortical mitochondria of *db/db* mice compared with *db/m* controls. Some results were unexpected, but may align with previous models of mitochondrial protection. These include changes to fuel substrates, reactive oxygen species (ROS) generation and oxygen availability per milligram of mitochondria. It is already hypothesised that metabolic changes in diabetes affect fuel preferences in renal proximal tubule cells [66]. Indeed, studies of PTEC metabolism indicate a switch to a reliance on fatty acid synthesis is a protective measure against the high glucose present in the proximal tubule cells under normal conditions [67]. With insulin resistance a decreased availability of intracellular glucose occurs in peripheral tissue, however, as renal proximal tubules are responsible for both gluconeogenesis and glucose recycling from the urinary ultrafiltrate, glucose uptake and release is increased in these cells under diabetic conditions [68–70]. Although CypD deletion induced changes in renal function in our first study, we did not find any statistically significant change in any renal functional parameter with Alisporivir treatment in our *db/db* model, although some trends were evident. However, the trend in body weight data for example is likely to be an artefact of randomisation and stochastic variation in *db/db* body size given the body composition and percentage fat mass remained consistent between treatment groups indicating mice were just smaller, not less obese. This is also demonstrated with the results of the CLAMS. Indeed, body size has been shown to be directly correlated with respiration, thus no real difference can be attributed to Alisporivir [20].

Some diabetes-associated mitochondrial changes, however, were altered with Alisporivir, indicating that some pharmacological activity was occurring in the renal cortex. Our data reveal that both mitochondrial function, and mitochondrial content, were altered in the diabetic kidney. All functional data were assessed per microgram of mitochondrial protein to confirm that these changes were a constitutive adaptation and did not simply reflect the increased mitochondrial content observed in renal tissue. Mitochondrial ETS components (citrate synthase activity, protein expression of ETS complexes) were also unchanged per microgram of protein between all groups. Calcium challenge induced rapid mitochondrial swelling in both *db/m* and *db/db* renal cortical mitochondria. This illustrates that some level of mitochondrial impairment was present in the renal mitochondria as a slower rate of swelling is generally observed in liver and cardiac mitochondria in other models [4,71,72]. However, CsA was able to effectively inhibit swelling in mitochondria isolated from *db/m* but not *db/db* mice. This abnormality in *db/db* mice was able to be rescued, with Alisporivir treatment able to partially restore mPTP inhibition. These data indicate that the drug was present in the renal cortical mitochondria, even though it did not alter OCR nor H_2O_2 production. CsA has been shown to reduce maximum respiration rates in a dose-dependent manner mediated through calcium sequestration, yet we did not see any respiration changes with Alisporivir at our dose [73].

It is possible that our data reveal that renal mitochondria are still able to adapt to chronic diabetes stressors via endogenous protective mechanisms. For example, previously elucidated adaptations in *db/db* mice include increased ROS generation mediated by ETS uncoupling [74]. One adaptation to this involves the up-regulation of Ucp-2 which is directly activated by the presence of ROS, and has been previously shown to act as a *positive* feedback brake on damaging ROS by uncoupling ETS activity [75]. In our study we observed an increase in OCR, paired with a concomitant decrease in radical sequestration in the production of H_2O_2. This indicates that mitochondrial uncoupling was occurring in the *db/db* mice. As we also observed an up-regulation of Ucp-2 gene expression, our data are consistent with this model and other studies demonstrating the protective nature of Ucp-2 from oxidative stress [76,77].

Finally, hypoxia is known to be a stressor of PTECs with decreased intrarenal oxygen levels previously demonstrated under diabetic conditions [78,79]. Although this was beyond the scope of our study, it is possible that adaptations to hypoxia may also be responsible for changes in ETS efficiency and ATP generation in addition to those shown here. Many factors influence the behaviour of CypD and the formation of the mPTP in a complex interactive network, however, targeting CypD with Alisporivir was unable to prevent the development of DKD in our *db/db* mice.

The present study has demonstrated that neither genetic deletion, nor partial blockade of CypD with Alisporivir, was able to rescue the common pathologies associated with progression of DKD. We conclude that CypD is an unsuitable target for rescuing mitochondrial heath in DKD. Although targeting mitochondrial function via inhibition of the mPTP has been demonstrated as an effective intervention in the pathophysiology of diseases in other organs, renal proximal tubular cells have a unique requirement for CypD under diabetic conditions and are unable to circumvent its physiological function to prevent mPTP-associated pathology.

Clinical Science (2020) **134** 239–259
https://doi.org/10.1042/CS20190787

Clinical perspectives

- Mitochondrial dysfunction, including enhanced susceptibility to mPTP, is an early event in the pathogenesis of DKD, however, the role of the mPTP and its activator, CypD, in DKD has not been fully explored.
- Genetic loss of CypD exacerbated diabetic renal injury, and treatment with a pharmacological inhibitor did not rescue mitochondrial function.
- CypD has a complex physiological and pathological role in the diabetic kidney which should be considered when treating DKD patients with CypD inhibitors.

Competing Interests

The authors declare that there are no competing interests associated with the manuscript.

Funding

This work was completed with support from: the Australian government Research Training Program [Scholarship (to R.S.J.L.)]; the Australian Diabetes Society [Skip Martin Early Career Fellowship (to M.T.C.)], M.T.C. is currently the recipient of a Career Development Award from JDRF Australia, Australian Research Council Special Research Initiative in Type 1 Juvenile Diabetes [grant number 4-CDA-2016-229-M-B]; the postdoctoral fellowship from JDRF [grant number 1-PDF-2017-421-A-N (to G.C.H.)]; and the National Health and Medical Research Council Research Fellows [grant number 1102935 (to J.M.F.) and grant number 1175760 (to M.E.C.)].

Open Access

Open access for this article was enabled by the participation of Monash University in an all-inclusive *Read & Publish* pilot with Portland Press and the Biochemical Society under a transformative agreement with CAUL.

Author Contribution

R.S.J.L. ran the animal studies, performed experiments, researched the data and co-wrote the paper. M.T.C. conceived the studies, ran the animal studies, researched the data and co-wrote the paper. G.C.H. ran the animal studies, performed experiments and provided intellectual input on the data. T.V.N., M.A., C.G., V.T.B., M.S., and J.M.F. performed experiments and assisted in researching and interpreting the data. D.C.H. and M.E.C. provided intellectual input on the data. All authors reviewed and edited the paper.

Acknowledgements

The authors would like to thank Sih Min Tan, Sally Penfold, Brooke Harcourt, Amy Morley and Karly Sourris for their technical assistance and also thank the Cellular and Molecular Metabolism Laboratory of the Baker Heart and Diabetes Institute, Melbourne, AU, for use of the CLAMs and EchoMRI equipment. We thank Carlos Rosado for assistance with generating PCR primers specifically for this project. We also acknowledge Georg Ramm, Joan Clark and Adam Costin of the Ramacciotti Centre for Cryo-electron Microscopy, at Monash University for technical assistance; and Monash Micro Imaging, for use of their equipment. We thank Novartis for providing the Alisporivir.

Abbreviations

A., Alisporivir treated mice; ATP, adenosine triphosphate; CIT, citrate (vehicle control); CKD, chronic kidney disease; Col IV, collagen type IV; CsA, cyclosporine A; *CypD*, cyclophilin D; *db*/*db*, diabetic, homozygous leptin receptor deficient ($Lepr^{db}$/$Lepr^{db}$); *db*/*m*, lean, heterozygous leptin receptor deficient ($Lepr^{db}$/$Lepr^{+}$); DKD, diabetic kidney disease; ETS, electron transport system; FAO, fatty acid oxidation; FCCP, carbonyl cyanide trifluoromethoxyphenylhydrazone; GSI, glomerular sclerosis index; H_2O_2, hydrogen peroxide; KIM-1, kidney injury molecule -1; mPT, mitochondrial permeability transition; mPTP, mitochondrial permeability transition pore; OCR, oxygen consumption rate; OXPHOS, oxidative phosphorylation; Ppif, peptidylprolyl isomerase F; PTEC, proximal tubular epithelial cell; RCR, respiratory control ratio; RER, respiratory exchange ratio; ROS, reactive oxygen species; RT-qPCR, quantitative reverse transcription-polymerase chain reaction; STZ, streptozotocin; V., vehicle control treated (10% Cremophor EL); WT, wild type.

References

1 Ogurtsova, K., da Rocha Fernandes, J.D., Huang, Y., Linnenkamp, U., Guariguata, L., Cho, N.H. et al. (2017) IDF diabetes atlas: global estimates for the prevalence of diabetes for 2015 and 2040. *Diabetes Res. Clin. Pract.* **128**, 40–50, https://doi.org/10.1016/j.diabres.2017.03.024
2 Brenner, B.M., Cooper, M.E., de Zeeuw, D., Keane, W.F., Mitch, W.E., Parving, H.H. et al. (2001) Effects of losartan on renal and cardiovascular outcomes in patients with type 2 diabetes and nephropathy. *N. Engl. J. Med.* **345**, 861–869, https://doi.org/10.1056/NEJMoa011161
3 Estacio, R.O., Jeffers, B.W., Gifford, N. and Schrier, R.W. (2000) Effect of blood pressure control on diabetic microvascular complications in patients with hypertension and type 2 diabetes. *Diabetes Care* **23**, B54–B64
4 Coughlan, M.T., Nguyen, T.V., Penfold, S.A., Higgins, G.C., Thallas-Bonke, V., Tan, S.M. et al. (2016) Mapping time-course mitochondrial adaptations in the kidney in experimental diabetes. *Clin. Sci.* **130**, 711–720, https://doi.org/10.1042/CS20150838
5 Duann, P. and Lin, P.H. (2017) Mitochondria damage and kidney disease. *Adv. Exp. Med. Biol.* **982**, 529–551, https://doi.org/10.1007/978-3-319-55330-6˙27
6 Blantz, R.C., Deng, A., Miracle, C.M. and Thomson, S.C. (2007) Regulation of kidney function and metabolism: a question of supply and demand. *Trans. Am. Clin. Climatol. Assoc.* **118**, 23–43
7 Sharma, K., Karl, B., Mathew, A.V., Gangoiti, J.A., Wassel, C.L., Saito, R. et al. (2013) Metabolomics reveals signature of mitochondrial dysfunction in diabetic kidney disease. *J. Am. Soc. Nephrol.* **24**, 1901–1912, https://doi.org/10.1681/ASN.2013020126
8 Wang, X., Zhang, X., Huang, Z., Wu, D., Liu, B., Zhang, R. et al. (2016) Protons trigger mitochondrial flashes. *Biophys. J.* **111**, 386–394, https://doi.org/10.1016/j.bpj.2016.05.052
9 Shang, W., Gao, H., Lu, F., Ma, Q., Fang, H., Sun, T. et al. (2016) Cyclophilin D regulates mitochondrial flashes and metabolism in cardiac myocytes. *J. Mol. Cell Cardiol.* **91**, 63–71, https://doi.org/10.1016/j.yjmcc.2015.10.036
10 Baines, C.P., Kaiser, R.A., Purcell, N.H., Blair, N.S., Osinska, H., Hambleton, M.A. et al. (2005) Loss of cyclophilin D reveals a critical role for mitochondrial permeability transition in cell death. *Nature* **434**, 658–662, https://doi.org/10.1038/nature03434
11 Nakagawa, T., Shimizu, S., Watanabe, T., Yamaguchi, O., Otsu, K., Yamagata, H. et al. (2005) Cyclophilin D-dependent mitochondrial permeability transition regulates some necrotic but not apoptotic cell death. *Nature* **434**, 652–658, https://doi.org/10.1038/nature03317
12 Kim, J.S., Qian, T. and Lemasters, J.J. (2003) Mitochondrial permeability transition in the switch from necrotic to apoptotic cell death in ischemic rat hepatocytes. *Gastroenterology* **124**, 494–503, https://doi.org/10.1053/gast.2003.50059
13 Karch, J., Kwong, J.Q., Burr, A.R., Sargent, M.A., Elrod, J.W., Peixoto, P.M. et al. (2013) Bax and Bak function as the outer membrane component of the mitochondrial permeability pore in regulating necrotic cell death in mice. *elife* **2**, e00772, https://doi.org/10.7554/eLife.00772
14 Karch, J. and Molkentin, J.D. (2014) Identifying the components of the elusive mitochondrial permeability transition pore. *Proc. Natl. Acad. Sci. U. S. A.* **111**, 10396–10397, https://doi.org/10.1073/pnas.1410104111
15 Waldmeier, P.C., Feldtrauer, J.J., Qian, T. and Lemasters, J.J. (2002) Inhibition of the mitochondrial permeability transition by the nonimmunosuppressive cyclosporin derivative NIM811. *Mol. Pharmacol.* **62**, 22–29, https://doi.org/10.1124/mol.62.1.22
16 Lin, D.T. and Lechleiter, J.D. (2002) Mitochondrial targeted cyclophilin D protects cells from cell death by peptidyl prolyl isomerization. *J. Biol. Chem.* **277**, 31134–31141, https://doi.org/10.1074/jbc.M112035200
17 Devalaraja-Narashimha, K., Diener, A.M. and Padanilam, B.J. (2009) Cyclophilin D gene ablation protects mice from ischemic renal injury. *Am. J. Physiol. Renal. Physiol.* **297**, F749–F759, https://doi.org/10.1152/ajprenal.00239.2009
18 Park, J.S., Pasupulati, R., Feldkamp, T., Roeser, N.F. and Weinberg, J.M. (2011) Cyclophilin D and the mitochondrial permeability transition in kidney proximal tubules after hypoxic and ischemic injury. *Am. J. Physiol. Renal. Physiol.* **301**, F134–F150, https://doi.org/10.1152/ajprenal.00033.2011
19 Hou, W., Leong, K.G., Ozols, E., Tesch, G.H., Nikolic-Paterson, D.J. and Ma, F.Y. (2018) Cyclophilin D promotes tubular cell damage and the development of interstitial fibrosis in the obstructed kidney. *Clin. Exp. Pharmacol. Physiol.* **45**, 250–260, https://doi.org/10.1111/1440-1681.12881
20 Lancaster, G.I. and Henstridge, D.C. (2018) Body composition and metabolic caging analysis in high fat fed mice. *J. Vis. Exp.*, https://doi.org/10.3791/57280
21 Saito, T., Sumithran, E., Glasgow, E.F. and Atkins, R.C. (1987) The enhancement of aminonucleoside nephrosis by the co-administration of protamine. *Kidney Int.* **32**, 691–699, https://doi.org/10.1038/ki.1987.262
22 Thallas-Bonke, V., Thorpe, S.R., Coughlan, M.T., Fukami, K., Yap, F.Y., Sourris, K.C. et al. (2008) Inhibition of NADPH oxidase prevents advanced glycation end product-mediated damage in diabetic nephropathy through a protein kinase C-alpha-dependent pathway. *Diabetes* **57**, 460–469, https://doi.org/10.2337/db07-1119
23 Frezza, C., Cipolat, S. and Scorrano, L. (2007) Organelle isolation: functional mitochondria from mouse liver, muscle and cultured fibroblasts. *Nat. Protoc.* **2**, 287–295, https://doi.org/10.1038/nprot.2006.478
24 Forbes, J.M., Ke, B.X., Nguyen, T.V., Henstridge, D.C., Penfold, S.A., Laskowski, A. et al. (2013) Deficiency in mitochondrial complex I activity due to Ndufs6 gene trap insertion induces renal disease. *Antioxid. Redox Signal.* **19**, 331–343, https://doi.org/10.1089/ars.2012.4719
25 Picard, M., White, K. and Turnbull, D.M. (2013) Mitochondrial morphology, topology, and membrane interactions in skeletal muscle: a quantitative three-dimensional electron microscopy study. *J. Appl. Physiol.* **114**, 161–171, https://doi.org/10.1152/japplphysiol.01096.2012
26 Granata, C., Oliveira, R.S., Little, J.P., Renner, K. and Bishop, D.J. (2016) Mitochondrial adaptations to high-volume exercise training are rapidly reversed after a reduction in training volume in human skeletal muscle. *FASEB J.* **30**, 3413–3423, https://doi.org/10.1096/fj.201500100R
27 Baines, C.P. and Gutiérrez-Aguilar, M. (2018) The still uncertain identity of the channel-forming unit(s) of the mitochondrial permeability transition pore. *Cell Calcium* **73**, 121–130, https://doi.org/10.1016/j.ceca.2018.05.003
28 Karch, J. and Molkentin, J.D. (2018) Identity of the elusive mitochondrial permeability transition pore: what it might be, what it was, and what it still could be. *Curr. Opin. Physiol.* **3**, 57–62, https://doi.org/10.1016/j.cophys.2018.03.001

Clinical Science (2020) **134** 239–259
https://doi.org/10.1042/CS20190787

29 Dhingra, R., Lieberman, B. and Kirshenbaum, L.A. (2019) Cyclophilin D phosphorylation is critical for mitochondrial calcium uniporter regulated permeability transition pore sensitivity. *Cardiovasc. Res.* **115**, 261–263, https://doi.org/10.1093/cvr/cvy270
30 Wang, X., Du, H., Shao, S., Bo, T., Yu, C., Chen, W. et al. (2018) Cyclophilin D deficiency attenuates mitochondrial perturbation and ameliorates hepatic steatosis. *Hepatology* **68**, 62–77, https://doi.org/10.1002/hep.29788
31 Porter, G.A. and Beutner, G. (2018) Cyclophilin D, somehow a master regulator of mitochondrial function. *Biomolecules* **8**, https://doi.org/10.3390/biom8040176
32 Luvisetto, S., Basso, E., Petronilli, V., Bernardi, P. and Forte, M. (2008) Enhancement of anxiety, facilitation of avoidance behavior, and occurrence of adult-onset obesity in mice lacking mitochondrial cyclophilin D. *Neuroscience* **155**, 585–596, https://doi.org/10.1016/j.neuroscience.2008.06.030
33 Elrod, J.W. and Molkentin, J.D. (2013) Physiologic functions of cyclophilin D and the mitochondrial permeability transition pore. *Circ. J.* **77**, 1111–1122, https://doi.org/10.1253/circj.CJ-13-0321
34 Radhakrishnan, J., Bazarek, S., Chandran, B. and Gazmuri, R.J. (2015) Cyclophilin-D: a resident regulator of mitochondrial gene expression. *FASEB J.* **29**, 2734–2748, https://doi.org/10.1096/fj.14-263855
35 Laker, R.C., Taddeo, E.P., Akhtar, Y.N., Zhang, M., Hoehn, K.L. and Yan, Z. (2016) The mitochondrial permeability transition pore regulator cyclophilin D exhibits tissue-specific control of metabolic homeostasis. *PLoS One* **11**, e0167910, https://doi.org/10.1371/journal.pone.0167910
36 Tavecchio, M., Lisanti, S., Bennett, M.J., Languino, L.R. and Altieri, D.C. (2015) Deletion of cyclophilin D impairs β-oxidation and promotes glucose metabolism. *Sci. Rep.* **5**, 15981, https://doi.org/10.1038/srep15981
37 Taddeo, E.P., Laker, R.C., Breen, D.S., Akhtar, Y.N., Kenwood, B.M., Liao, J.A. et al. (2014) Opening of the mitochondrial permeability transition pore links mitochondrial dysfunction to insulin resistance in skeletal muscle. *Mol. Metab.* **3**, 124–134, https://doi.org/10.1016/j.molmet.2013.11.003
38 Antoniel, M., Giorgio, V., Fogolari, F., Glick, G.D., Bernardi, P. and Lippe, G. (2014) The oligomycin-sensitivity conferring protein of mitochondrial ATP synthase: emerging new roles in mitochondrial pathophysiology. *Int. J. Mol. Sci.* **15**, 7513–7536, https://doi.org/10.3390/ijms15057513
39 Giorgio, V., Bisetto, E., Soriano, M.E., Dabbeni-Sala, F., Basso, E., Petronilli, V. et al. (2009) Cyclophilin D modulates mitochondrial F0F1-ATP synthase by interacting with the lateral stalk of the complex. *J. Biol. Chem.* **284**, 33982–33988, https://doi.org/10.1074/jbc.M109.020115
40 Chinopoulos, C., Konràd, C., Kiss, G., Metelkin, E., Töröcsik, B., Zhang, S.F. et al. (2011) Modulation of F0F1-ATP synthase activity by cyclophilin D regulates matrix adenine nucleotide levels. *FEBS J.* **278**, 1112–1125, https://doi.org/10.1111/j.1742-4658.2011.08026.x
41 Bernardi, P. (2018) Why F-ATP synthase remains a strong candidate as the mitochondrial permeability transition pore. *Front. Physiol.* **9**, 1543, https://doi.org/10.3389/fphys.2018.01543
42 Giorgio, V., Soriano, M.E., Basso, E., Bisetto, E., Lippe, G., Forte, M.A. et al. (2010) Cyclophilin D in mitochondrial pathophysiology. *Biochim. Biophys. Acta* **1797**, 1113–1118, https://doi.org/10.1016/j.bbabio.2009.12.006
43 Yan, S., Du, F., Wu, L., Zhang, Z., Zhong, C., Yu, Q. et al. (2016) F1F0 ATP synthase-cyclophilin D interaction contributes to diabetes-induced synaptic dysfunction and cognitive decline. *Diabetes* **65**, 3482–3494, https://doi.org/10.2337/db16-0556
44 Klawitter, J., Pennington, A., Klawitter, J., Thurman, J.M. and Christians, U. (2017) Mitochondrial cyclophilin D ablation is associated with the activation of Akt/p70S6K pathway in the mouse kidney. *Sci. Rep.* **7**, 10540, https://doi.org/10.1038/s41598-017-10076-9
45 Simon, N. and Hertig, A. (2015) Alteration of fatty acid oxidation in tubular epithelial cells: from acute kidney injury to renal fibrogenesis. *Front. Med.* **2**, 52, https://doi.org/10.3389/fmed.2015.00052
46 Kang, H.M., Ahn, S.H., Choi, P., Ko, Y.A., Han, S.H., Chinga, F. et al. (2015) Defective fatty acid oxidation in renal tubular epithelial cells has a key role in kidney fibrosis development. *Nat. Med.* **21**, 37–46, https://doi.org/10.1038/nm.3762
47 Proctor, G., Jiang, T., Iwahashi, M., Wang, Z., Li, J. and Levi, M. (2006) Regulation of renal fatty acid and cholesterol metabolism, inflammation, and fibrosis in Akita and OVE26 mice with type 1 diabetes. *Diabetes* **55**, 2502–2509, https://doi.org/10.2337/db05-0603
48 Halestrap, A.P., Connern, C.P., Griffiths, E.J. and Kerr, P.M. (1997) Cyclosporin A binding to mitochondrial cyclophilin inhibits the permeability transition pore and protects hearts from ischaemia/reperfusion injury. *Mol. Cell. Biochem.* **174**, 167–172, https://doi.org/10.1023/A:1006879618176
49 Gomez, L., Thibault, H., Gharib, A., Dumont, J.M., Vuagniaux, G., Scalfaro, P. et al. (2007) Inhibition of mitochondrial permeability transition improves functional recovery and reduces mortality following acute myocardial infarction in mice. *Am. J. Physiol. Heart Circ. Physiol.* **293**, H1654–H1661, https://doi.org/10.1152/ajpheart.01378.2006
50 Hansson, M.J., Mattiasson, G., Månsson, R., Karlsson, J., Keep, M.F., Waldmeier, P. et al. (2004) The nonimmunosuppressive cyclosporin analogs NIM811 and UNIL025 display nanomolar potencies on permeability transition in brain-derived mitochondria. *J. Bioenerg. Biomembr.* **36**, 407–413, https://doi.org/10.1023/B:JOBB.0000041776.31885.45
51 Flisiak, R., Horban, A., Gallay, P., Bobardt, M., Selvarajah, S., Wiercinska-Drapalo, A. et al. (2008) The cyclophilin inhibitor Debio-025 shows potent anti-hepatitis C effect in patients coinfected with hepatitis C and human immunodeficiency virus. *Hepatology* **47**, 817–826, https://doi.org/10.1002/hep.22131
52 Gallay, P.A. and Lin, K. (2013) Profile of alisporivir and its potential in the treatment of hepatitis C. *Drug Des. Devel. Ther.* **7**, 105–115, https://doi.org/10.2147/DDDT.S30946
53 Quarato, G., D'Aprile, A., Gavillet, B., Vuagniaux, G., Moradpour, D., Capitanio, N. et al. (2012) The cyclophilin inhibitor alisporivir prevents hepatitis C virus-mediated mitochondrial dysfunction. *Hepatology* **55**, 1333–1343, https://doi.org/10.1002/hep.25514
54 Paeshuyse, J., Kaul, A., De Clercq, E., Rosenwirth, B., Dumont, J.M., Scalfaro, P. et al. (2006) The non-immunosuppressive cyclosporin DEBIO-025 is a potent inhibitor of hepatitis C virus replication in vitro. *Hepatology* **43**, 761–770, https://doi.org/10.1002/hep.21102
55 Ederoth, P., Grins, E., Dardashti, A., Brondén, B., Metzsch, C., Erdling, A. et al. (2016) Ciclosporin to protect renal function in cardiac surgery (CiPRICS): a study protocol for a double-blind, randomised, placebo-controlled, proof-of-concept study. *BMJ Open* **6**, e012299
56 Piot, C., Croisille, P., Staat, P., Thibault, H., Rioufol, G., Mewton, N. et al. (2008) Effect of cyclosporine on reperfusion injury in acute myocardial infarction. *N. Engl. J. Med.* **359**, 473–481, https://doi.org/10.1056/NEJMoa071142

57 Cung, T.T., Morel, O., Cayla, G., Rioufol, G., Garcia-Dorado, D., Angoulvant, D. et al. (2015) Cyclosporine before PCI in patients with acute myocardial infarction. *N. Engl. J. Med.* **373**, 1021–1031, https://doi.org/10.1056/NEJMoa1505489
58 Rahman, F.A., Abdullah, S.S., Manan, WZWA, Tan, L.T., Neoh, C.F., Ming, L.C. et al. (2018) Efficacy and safety of cyclosporine in acute myocardial infarction: a systematic review and meta-analysis. *Front. Pharmacol.* **9**, 238, https://doi.org/10.3389/fphar.2018.00238
59 Schiavone, M., Zulian, A., Menazza, S., Petronilli, V., Argenton, F., Merlini, L. et al. (2017) Alisporivir rescues defective mitochondrial respiration in Duchenne muscular dystrophy. *Pharmacol. Res.* **125**, 122–131, https://doi.org/10.1016/j.phrs.2017.09.001
60 Palma, E., Tiepolo, T., Angelin, A., Sabatelli, P., Maraldi, N.M., Basso, E. et al. (2009) Genetic ablation of cyclophilin D rescues mitochondrial defects and prevents muscle apoptosis in collagen VI myopathic mice. *Hum. Mol. Genet.* **18**, 2024–2031, https://doi.org/10.1093/hmg/ddp126
61 Wu, Q., Wang, X., Nepovimova, E., Wang, Y., Yang, H. and Kuca, K. (2018) Mechanism of cyclosporine A nephrotoxicity: oxidative stress, autophagy, and signalings. *Food Chem. Toxicol.* **118**, 889–907, https://doi.org/10.1016/j.fct.2018.06.054
62 Strzelecki, T., Kumar, S., Khauli, R. and Menon, M. (1988) Impairment by cyclosporine of membrane-mediated functions in kidney mitochondria. *Kidney Int.* **34**, 234–240, https://doi.org/10.1038/ki.1988.170
63 Lee, S.H., Yoon, Y.C., Jang, Y.Y., Song, J.H., Han, E.S. and Lee, C.S. (2001) Effect of iron and ascorbate on cyclosporine-induced oxidative damage of kidney mitochondria and microsomes. *Pharmacol. Res.* **43**, 161–171, https://doi.org/10.1006/phrs.2000.0759
64 Kuroyanagi, Y., Gotoh, Y., Kasahara, K., Nagano, C., Fujita, N., Yamakawa, S. et al. (2018) Effectiveness and nephrotoxicity of a 2-year medium dose of cyclosporine in pediatric patients with steroid-dependent nephrotic syndrome: determination of the need for follow-up kidney biopsy. *Clin. Exp. Nephrol.* **22**, 413–419, https://doi.org/10.1007/s10157-017-1444-3
65 Burdmann, E.A., Andoh, T.F., Yu, L. and Bennett, W.M. (2003) Cyclosporine nephrotoxicity. *Semin. Nephrol.* **23**, 465–476, https://doi.org/10.1016/S0270-9295(03)00090-1
66 Rosca, M.G., Vazquez, E.J., Chen, Q., Kerner, J., Kern, T.S. and Hoppel, C.L. (2012) Oxidation of fatty acids is the source of increased mitochondrial reactive oxygen species production in kidney cortical tubules in early diabetes. *Diabetes* **61**, 2074–2083, https://doi.org/10.2337/db11-1437
67 Uchida, S. and Endou, H. (1988) Substrate specificity to maintain cellular ATP along the mouse nephron. *Am. J. Physiol.* **255**, F977–F983
68 Meyer, C., Stumvoll, M., Dostou, J., Welle, S., Haymond, M. and Gerich, J. (2002) Renal substrate exchange and gluconeogenesis in normal postabsorptive humans. *Am. J. Physiol. Endocrinol. Metab.* **282**, E428–E434, https://doi.org/10.1152/ajpendo.00116.2001
69 Stumvoll, M., Meyer, C., Mitrakou, A., Nadkarni, V. and Gerich, J.E. (1997) Renal glucose production and utilization: new aspects in humans. *Diabetologia* **40**, 749–757, https://doi.org/10.1007/s001250050745
70 Alsahli, M. and Gerich, J.E. (2017) Renal glucose metabolism in normal physiological conditions and in diabetes. *Diabetes Res. Clin. Pract.* **133**, 1–9, https://doi.org/10.1016/j.diabres.2017.07.033
71 Sourris, K.C., Harcourt, B.E., Tang, P.H., Morley, A.L., Huynh, K., Penfold, S.A. et al. (2012) Ubiquinone (coenzyme Q10) prevents renal mitochondrial dysfunction in an experimental model of type 2 diabetes. *Free Radic. Biol. Med.* **52**, 716–723, https://doi.org/10.1016/j.freeradbiomed.2011.11.017
72 Borillo, G.A., Mason, M., Quijada, P., Völkers, M., Cottage, C., McGregor, M. et al. (2010) Pim-1 kinase protects mitochondrial integrity in cardiomyocytes. *Circ. Res.* **106**, 1265–1274, https://doi.org/10.1161/CIRCRESAHA.109.212035
73 Fournier, N., Ducet, G. and Crevat, A. (1987) Action of cyclosporine on mitochondrial calcium fluxes. *J. Bioenerg. Biomembr.* **19**, 297–303, https://doi.org/10.1007/BF00762419
74 Persson, M.F., Franzén, S., Catrina, S.B., Dallner, G., Hansell, P., Brismar, K. et al. (2012) Coenzyme Q10 prevents GDP-sensitive mitochondrial uncoupling, glomerular hyperfiltration and proteinuria in kidneys from db/db mice as a model of type 2 diabetes. *Diabetologia* **55**, 1535–1543, https://doi.org/10.1007/s00125-012-2469-5
75 Brand, M.D., Affourtit, C., Esteves, T.C., Green, K., Lambert, A.J., Miwa, S. et al. (2004) Mitochondrial superoxide: production, biological effects, and activation of uncoupling proteins. *Free Radic. Biol. Med.* **37**, 755–767, https://doi.org/10.1016/j.freeradbiomed.2004.05.034
76 Friederich, M., Fasching, A., Hansell, P., Nordquist, L. and Palm, F. (2008) Diabetes-induced up-regulation of uncoupling protein-2 results in increased mitochondrial uncoupling in kidney proximal tubular cells. *Biochim. Biophys. Acta* **1777**, 935–940, https://doi.org/10.1016/j.bbabio.2008.03.030
77 Chen, X.L., Tang, W.X., Tang, X.H., Qin, W. and Gong, M. (2014) Downregulation of uncoupling protein-2 by genipin exacerbates diabetes-induced kidney proximal tubular cells apoptosis. *Ren. Fail.* **36**, 1298–1303, https://doi.org/10.3109/0886022X.2014.930650
78 Palm, F., Cederberg, J., Hansell, P., Liss, P. and Carlsson, P.O. (2003) Reactive oxygen species cause diabetes-induced decrease in renal oxygen tension. *Diabetologia* **46**, 1153–1160, https://doi.org/10.1007/s00125-003-1155-z
79 Friederich-Persson, M., Thörn, E., Hansell, P., Nangaku, M., Levin, M. and Palm, F. (2013) Kidney hypoxia, attributable to increased oxygen consumption, induces nephropathy independently of hyperglycemia and oxidative stress. *Hypertension* **62**, 914–919, https://doi.org/10.1161/HYPERTENSIONAHA.113.01425